

# Global Biogeochemical Cycles®



## RESEARCH ARTICLE

10.1029/2024GB008439

### Key Points:

- N<sub>2</sub>O net emissions from the permafrost region increased from 1969 to 2019 due to warming and permafrost degradation
- Natural terrestrial ecosystems act as net sinks or sources of N<sub>2</sub>O ranging from −12 to 900 mg N m<sup>−2</sup> yr<sup>−1</sup> in this region
- N<sub>2</sub>O emissions from thawing permafrost increase from 0 to 925 mg N m<sup>−2</sup> yr<sup>−1</sup>, with a mean of 3.35 and median of 0.97 mg N m<sup>−2</sup> yr<sup>−1</sup>

### Supporting Information:

Supporting Information may be found in the online version of this article.

### Correspondence to:

Q. Zhuang,  
qzhuang@purdue.edu

### Citation:

Yuan, Y., Zhuang, Q., Zhao, B., & Shurpali, N. (2025). Impacts of permafrost degradation on N<sub>2</sub>O emissions from natural terrestrial ecosystems in northern high latitudes: A process-based biogeochemistry model analysis. *Global Biogeochemical Cycles*, 39, e2024GB008439. <https://doi.org/10.1029/2024GB008439>

Received 21 NOV 2024  
Accepted 4 APR 2025

## Impacts of Permafrost Degradation on N<sub>2</sub>O Emissions From Natural Terrestrial Ecosystems in Northern High Latitudes: A Process-Based Biogeochemistry Model Analysis

Ye Yuan<sup>1</sup> , Qianlai Zhuang<sup>1,2</sup> , Bailu Zhao<sup>1</sup> , and Narasinha Shurpali<sup>3</sup>

<sup>1</sup>Department of Earth, Atmospheric, and Planetary Science, Purdue University, West Lafayette, IN, USA, <sup>2</sup>Department of Agronomy, Purdue University, West Lafayette, IN, USA, <sup>3</sup>Natural Resources Institute Finland (Luke), Maaninka, Finland

**Abstract** Nitrous oxide (N<sub>2</sub>O) is a potent greenhouse gas with its radiative forcing 265–298 times stronger than that of carbon dioxide (CO<sub>2</sub>). Recent field studies show N<sub>2</sub>O emissions from northern high latitude (north of 45°N) ecosystems have increased due to warming. However, spatiotemporal quantification of N<sub>2</sub>O emissions remains inadequate in this region. Here we revise the Terrestrial Ecosystem Model to incorporate more detailed processes of soil nitrogen (N) biogeochemical cycling, permafrost thawing effects, and atmospheric N deposition. Terrestrial Ecosystem Model is then used to analyze N<sub>2</sub>O emissions from natural terrestrial ecosystems in the region. Our study reveals that regional N<sub>2</sub>O production and net emissions increased from 1969 to 2019. Production rose from 1.12 (0.82–1.46) to 1.18 (0.84–1.51) Tg N yr<sup>−1</sup>, while net emissions increased from 0.98 (0.7–1.34) to 1.05 (0.72–1.39) Tg N yr<sup>−1</sup>, considering permafrost thawing. Emissions from permafrost regions grew from 0.37 (0.2–0.57) to 0.41 (0.21–0.6) Tg N yr<sup>−1</sup>. Soil N<sub>2</sub>O uptake from the atmosphere remained relatively stable at 0.12 (0.1–0.15) Tg N yr<sup>−1</sup>. Atmospheric N deposition significantly increased N<sub>2</sub>O emission by 37.2 ± 2.9%. Spatially, natural terrestrial ecosystems act as net sources or sinks of −12 to 900 mg N m<sup>−2</sup> yr<sup>−1</sup> depending on changing temperature, precipitation, soil characteristics, and vegetation types. Our findings underscore the critical need for more observational studies to reduce the uncertainty in N<sub>2</sub>O budget.

## 1. Introduction

Global climate change entails rising air temperatures, a change in precipitation patterns, and a more frequent occurrence of extreme weather events. The prevailing consensus is that temperature increase will be most pronounced in the northern high latitudes (Overland et al., 2014). The Arctic has already warmed to more than 2°C above the preindustrial levels, and this rapid warming is expected to double by the middle of this century (Natali et al., 2021; Post et al., 2019). The northern high latitude (north of 45°N) land areas are predicted to warm up to 3–7°C by the end of this century (IPCC, 2013), leading to widespread permafrost degradation and thaw (Borge et al., 2017; Jones et al., 2016; Romanovsky et al., 2010) and substantial changes in ecosystem functioning (Grosse et al., 2016) and microbial activities (Monteux et al., 2020). These changes are projected to accelerate the decomposition of permafrost soil organic matter (SOM) and stimulate greenhouse gas (GHG) emissions (Natali et al., 2021; Sierra et al., 2015; Voigt et al., 2017; Yang et al., 2010). The actual area underlain by permafrost covers approximately 14 million km<sup>2</sup>, constituting about 15% of the exposed land surface area in the Northern Hemisphere, while a majority of this area is in the northern high latitudes (Obu, 2021), accounting for 32.5% (13.2 × 10<sup>6</sup> km<sup>2</sup>) of northern high latitude land area (Brown et al., 2002). Permafrost soils are also large nitrogen (N) reservoirs (Post et al., 1985), with a conservative estimate of 55–67 Pg N in the upper 3 m and 21 Pg N in the upper 1m (Harden et al., 2012; Palmtag et al., 2022) soil layer. Experimental permafrost thawing with snow fences has shown that the nitrogen availability increases in tundra ecosystems (Salmon et al., 2016).

While past studies on GHG emissions from the northern high latitudes have mainly focused on carbon-based compounds, recent studies have shown that soils might also be a significant source of N<sub>2</sub>O from peatlands (Marushchak et al., 2011; Repo et al., 2009), with high N<sub>2</sub>O production potential in soils after permafrost thaw (Elberling et al., 2010). Elevated soil N<sub>2</sub>O concentrations have been observed in upland tundra due to thawing permafrost (Abbott & Jones, 2015). Furthermore, rising temperatures also promote N<sub>2</sub>O emissions from tundra ecosystems, including both upland tundra and vegetated peat plateau complexes (Voigt et al., 2017), which cover 8% of the global land surface (McGuire et al., 2012) and 17.9% of the northern high latitudes (Melillo et al., 1993). However, how permafrost thaw affects N<sub>2</sub>O emissions by potentially unlocking the vast N stocks currently stored

© 2025. The Author(s).

This is an open access article under the terms of the [Creative Commons Attribution License](https://creativecommons.org/licenses/by/4.0/), which permits use, distribution and reproduction in any medium, provided the original work is properly cited.

in soils is not yet explored (Harden et al., 2012). Although the northern high latitude  $N_2O$  fluxes are low on a mass basis, they are important since  $N_2O$  is a more potent GHG with a radiative forcing of 265–298 times stronger than that of  $CO_2$  (IPCC, 2013).  $N_2O$  contributes nearly 10% of the total anthropogenic radiative forcing and is among the key chemicals destroying the stratospheric ozone layer (Ravishankara et al., 2009).

Soil temperature, moisture, acidity, SOM content, C/N ratio, and plant growth have been identified as the key regulators of  $N_2O$  emissions from cold soils (Marushchak et al., 2011; Smith et al., 1998; Voigt et al., 2017). Soil temperature is a key factor in both organic (e.g., decomposition) and inorganic processes (e.g., mineralization) in the N cycle (Conant et al., 2011; Dai et al., 2020). Soil moisture determines soil oxygen availability. High water content leads to low oxygen condition, which is associated with an anaerobic environment, whereas less water leads to an oxidizing environment. The soil oxygen condition influences microorganism activities, thus the nitrification and denitrification rates (Bateman & Baggs, 2005). Soil acidity controls the chemical reactions involving  $H^+$  or  $OH^-$ , both of which influence the activity of microorganisms and enzymes (Kunhikrishnan et al., 2016). Traditionally,  $N_2O$  emissions originating from areas of high latitudes were viewed as an insignificant source (Martikainen et al., 1993; Potter et al., 1996) due to a slow mineralization rate under low temperature, humid conditions, and low atmospheric deposition of nitrogen (Dentener et al., 2006). In natural terrestrial ecosystems of northern high latitudes, the limited shortage of mineral N used to be one of the main reasons for the low nitrous oxide ( $N_2O$ ) emissions measured from tundra soils (Ludwig et al., 2006; Ma et al., 2007). However, in recent decades, the warming climate and loss of permafrost may disrupt the past closed N cycling and cause significant export of inorganic N (Frey et al., 2007; Hansen & Elberling, 2023; Marushchak et al., 2021; McClelland et al., 2007). Such patterns may result from the introduction of previously frozen N into the cycling pool due to gradual degradation of permafrost that deepens the zone of seasonally thawed soils, or from direct effects of temperature on microbial processes.

The net  $N_2O$  emissions at the soil surface are the result of gross  $N_2O$  production, uptake, and consumption, which are co-occurring processes.  $N_2O$  consumption occurs when soil water content increases and oxygen content decreases, and soils transition from aerobic to anaerobic conditions. Soil water or oxygen content, mineralization, temperature, soil pH, and concentrations of electron donors and acceptors all influence soil  $N_2O$  uptake (Chapuis-Lardy et al., 2007; Wen et al., 2016). In northern high latitudes, negative  $N_2O$  fluxes are observed at various ecosystems, particularly in dry soils (where nitrification is dominant), continuously flooding soils (where complete denitrification occurs, with  $N_2$  as the main product), or in soils with low N concentration (Butterbach-Bahl et al., 1998; Cantarel et al., 2011; Cui et al., 2018; Goldberg & Gebauer, 2009; Gong et al., 2019; Groffman et al., 2006; Matson et al., 2009; Morishita et al., 2014; Takakai et al., 2008; Teepe, Vor, et al., 2004; Ullah & Moore, 2011; Wu et al., 2019; Zhou et al., 2016).

Over the past century, anthropogenic activities have doubled fixed nitrogen levels (Fowler et al., 2013), with a continuous increase observed in recent years due to agricultural and industrial practices (Vishwakarma et al., 2023). A significant portion of this anthropogenic nitrogen enters ecosystems, including the natural terrestrial ecosystems in the northern high latitudes, through atmospheric deposition (Ackerman et al., 2019), thereby causing profound alterations in ecosystem processes, nitrogen cycling, and GHG emissions.

To date, a group of process-based biogeochemistry models have been used to quantify  $N_2O$  fluxes, including a version of Terrestrial Ecosystem Model (TEM) (Qin et al., 2014, 2015; Yu & Zhuang, 2019), the Community Land Model, Carbon and Nitrogen cycles (CLM-CN) (Saikawa et al., 2013), the daily Century (DayCent) model (Del Grosso et al., 2000; Parton et al., 1996), and the Denitrification/Decomposition (DNDC) Model (Li, 1992). More recently, the TEM QUINCY (Quantifying Interactions between terrestrial Nutrient Cycles and the climate system) accounted for the effects of soil freezing and thawing to study the effects of increased nutrient availability on plant growth and  $N_2O$  emission at the site level, and find that nitrogen released from permafrost thaw provides only a modest fertilization effect on plant growth, due to a timing mismatch between nitrogen release and plant uptake but leads to increased  $N_2O$  emissions and nitrogen leaching into downstream rivers (Lacroix et al., 2022). However, none of these has combined the permafrost thawing effects on  $N_2O$  emission and uptake from the atmosphere. Quantification of the  $N_2O$  emission across the whole northern high latitudes is still outstanding. Here we further develop the biogeochemistry model TEM based on the version of Yu and Zhuang (2019) by incorporating the effects of permafrost thawing on the nitrogen cycle, latest spatially explicit and depth-resolved permafrost C/N stocks, the soil  $N_2O$  uptake from the atmosphere, and the atmospheric nitrogen deposition. The revised TEM is calibrated and validated and then applied to quantify  $N_2O$  emissions from the natural

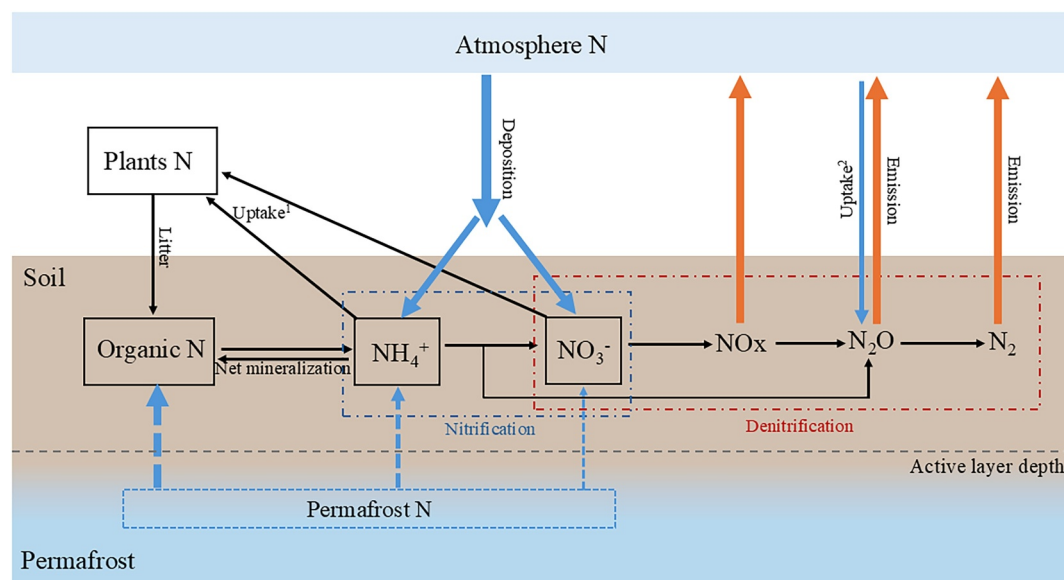


**Figure 1.** Nitrogen cycle and  $N_2O$  production in the revised Terrestrial Ecosystem Model. Blue arrows represent nitrogen (N) inputs, while orange arrows represent nitrogen outputs. The active layer depth varies over time. Net mineralization: The difference between mineralization (organic N mineralized to inorganic N) and immobilization (inorganic N to organic N); Litter: organic N from plant litters; Uptake<sup>1</sup>: inorganic N uptake by plants; Deposition: atmospheric deposition of N; Emission:  $N_2O$  emissions from soils; Uptake<sup>2</sup>: Atmospheric  $N_2O$  uptake in soils.

terrestrial ecosystems in the northern high latitudes (north of 45°N, including both permafrost and non-permafrost areas) from 1969 to 2019.

## 2. Method

### 2.1. Model Description

Terrestrial Ecosystem Model is a global-scale biogeochemical model designed to quantify the cycling of carbon (C) and nitrogen (N) in terrestrial ecosystems (McGuire et al., 1997; Melillo et al., 1993; Zhuang et al., 2003). The major processes of nitrogen (N) dynamic module were inherited from McGuire et al. (1997) and Yu and Zhuang (2019), including nitrogen input from plant litters, nitrogen uptake by vegetation, net soil mineralization, nitrogen lost from ecosystem, as well as the principles of the stoichiometry of carbon and nitrogen dynamics in soils. Detailed equations can be found in McGuire et al. (1997) and Yu and Zhuang (2019). Here we revised the N cycling algorithms in TEM by enhancing the representation of physical effects on nitrification and denitrification modeling and incorporating the loss of nitrogen through gas emissions with empirical equations, the uptake of  $N_2O$  from the atmosphere, and additional inputs of total nitrogen and organic carbon resulting from permafrost thawing, and atmospheric N deposition (Figure 1 and Equations 1–12).

The net  $N_2O$  emission ( $N_2O_{emi}$ ) is calculated as the difference between  $N_2O$  production ( $N_2O_{pro}$ ) in soils and soil  $N_2O$  uptake ( $N_2O_{upt}$ ) from the atmosphere (Equation 1). We incorporate  $N_2O$  originating from nitrification ( $N_2O_N$ ) and denitrification ( $N_2O_{DN}$ ) into the total  $N_2O$  production (Equation 2):

$$N_2O_{emi} = N_2O_{pro} - N_2O_{upt} \quad (1)$$

$$N_2O_{pro} = N_2O_N + N_2O_{DN} \quad (2)$$

The amount of  $N_2O$  uptake ( $N_2O_{upt}$ ) was calculated according to Fick's law of gas diffusion (Equation 3), where  $C_{air}$  and  $C_{soil}$  represent  $N_2O$  concentration in air and soils, respectively. We used atmospheric  $N_2O$  concentrations of 331.1 ppb.  $k_s$  represents the diffusion coefficient. The  $N_2O$  diffusion coefficient used in this study is  $1.26 \times 10^{-6} \text{ m}^2 \text{ s}^{-1}$  (van Bochove, Bertran, & Caron, 1998). We assume that the produced  $N_2O$  accumulates

within the top 30 cm of the soil before emitting into the atmosphere. Therefore, the calculation of soil gas concentration is derived by dividing the  $N_2O$  produced in a  $1\text{ m}^2$  area by the 30 cm height of the soil layer.

$$N_2O_{\text{upt}} = (C_{\text{air}} - C_{\text{soil}}) k_s \quad (3)$$

The  $N_2O$  production rate from nitrification ( $N_2O_N$ ) was determined by  $k_n$ , the fraction of the nitrified N lost, which is 0.02 in the DayCent model (Delgrosso et al., 2000; Parton et al., 1996), and 0.0006 in the DNDC Model (Li, 1992), and the nitrification rate  $N_{\text{nit}}$  (Equation 4). In this study, we calibrated  $k_n$  within the range of 0.0006–0.02 using observational data. The nitrification rate algorithm (Equation 5) is based on Parton et al. (2001), where  $k_f$  represents the fraction of net mineralization to be nitrified,  $N_{\text{min}}$  is the net mineralization rate,  $k_{\text{max}}$  is the maximum fraction of  $NH_4^+$  nitrified, and  $NH_4^+$  is the model-derived soil ammonium concentration ( $\text{g N m}^{-2}$ ). The factors  $f_m$ ,  $f_{mn}$ , and  $f_{phn}$  account for the effects of temperature, soil moisture, and soil pH, respectively. Detailed equations can be found in Huang and Gerber (2015), Parton et al. (1996), and Parton et al. (2001).

$$N_2O_N = k_n N_{\text{nit}} \quad (4)$$

$$N_{\text{nit}} = k_1 N_{\text{min}} + k_{\text{max}} (NH_4^+) f_m f_{mn} f_{phn} \quad (5)$$

The  $N_2O$  production rate ( $N_2O_{\text{DN}}$ ) from denitrification was determined by the denitrification rate ( $N_{\text{deni}}$ ) and  $k_{dn}$ , the fraction of denitrified N lost as  $N_2O$  fluxes (Equation 6).  $N_{\text{deni}}$  represents the denitrification rate (Equation 7), which relates nitrogen gas flux to soil respiration ( $CO_2$ ) and nitrate levels ( $NO_3$ ).  $f_{no3k}$  and  $f_{co2k}$  are related coefficients, and the effects of soil temperature ( $f_{idn}$ ), moisture ( $f_{mdn}$ ), and pH ( $f_{phdn}$ ). These functions are derived from Del Grosso et al. (2000), Hénault et al. (2005), and Wagena et al. (2017).  $k_{dn}$  is calculated based on the ratio of  $N_2$  to the sum of  $N_2$  and  $N_2O$  ( $N_2/(N_2+N_2O)$ ,  $r_{n2}$ ) from denitrification (Equation 8), which is influenced by soil moisture ( $f_m$ ), pH ( $f_{phm2}$ ) and electron level ( $f_{nc}$ , Equation 9). The pH function for  $N_2/N_2O$  ratio ( $f_{phm2}$ ) is derived from the SWAT model (Wagena et al., 2017) (Equation 10). The effects of electron donor to the substrate ( $f_{nc}$ , Equation 11) and water function to  $N_2$  ratio ( $f_m$ , Equation 12) are derived from Del Grosso et al. (2000), in which  $k_{gc}$  represents soil gas diffusivity coefficient, calculated as a function of porosity and field capacity;  $NO_3/CO_2$  represents the ratio of  $NO_3$  to heterotrophic  $CO_2$  respiration;  $wfps$  represents water filled pore space.

$$N_2O_{\text{DN}} = k_{dn} N_{\text{deni}} \quad (6)$$

$$N_{\text{deni}} = \begin{cases} f_{no3k} NO_3^{0.57} f_{idn} f_{mdn} f_{phdn}, & (NO_3 \leq CO_2) \\ f_{co2k} CO_2^{1.3} f_{idn} f_{mdn} f_{phdn}, & (NO_3 > CO_2) \end{cases} \quad (7)$$

$$k_{dn} = \frac{1}{1 + r_{n2}} \quad (8)$$

$$r_{n2} = f_{nc} f_m f_{phm2} \quad (9)$$

$$f_{phm2} = \begin{cases} 0.1, & (pH \leq 4.5) \\ \frac{1}{1470e^{-1.1pH}}, & (pH > 4.5) \end{cases} \quad (10)$$

$$f_{nc} = \max \left( k_{gc} e^{\left(-0.8 \frac{NO_3}{CO_2}\right)}, 0.16 k_{gc} \right) \quad (11)$$

$$f_m = \max (0.1, 0.015 wfps - 0.32) \quad (12)$$

To assess the impact of permafrost thawing on N mineralization, we accounted for the additional nitrogen and carbon input due to permafrost thaw depth changes. The thawing depth is calculated monthly. Each month's thaw depth for the current year is compared to the maximum thaw depth from prior years, beginning from 1969, which always reaches its peak during summer. If the thawing depth in the current month exceeds the previous maximum thawing depth, the thawing depth difference is considered the change in thawing depth, and the total N and

organic C between the two depths were added to soil C and N cycle pools. Conversely, if the thawing depth in the current month is less than the previous maximum, the carbon and nitrogen in previously thawed layers are used. We based our calculation of thawing depth on a soil thermal model, which is tested effectively against the observations. Detailed information is well documented in Liu et al. (2022) and Zhuang et al. (2001). We utilized the latest spatially explicit northern permafrost soil carbon and nitrogen dataset (Palmtag et al., 2022), which provides the vertical and horizontal distributions of organic carbon and total nitrogen stocks at depths of 0–30 cm, 30–50 cm, 50–100 cm, 100–200 cm, and 200–300 cm at 300 m pixel resolution. This dataset was resampled to  $0.5^\circ \times 0.5^\circ$  grid cells for model input. The maximum soil depth was set to 13 m (Tao et al., 2019; Liu et al., 2022). For depths beyond 300 cm, we assumed that carbon and nitrogen stocks follow the distribution in the 200–300 cm layer. Based on the mineral nitrogen to total nitrogen ratios reported by Marushchak et al. (2021) and Beermann et al. (2017), we estimated that 98% of total nitrogen is organic, which was added to the soil organic nitrogen pool for mineralization. We further assumed that 1.8% of total nitrogen is  $\text{NH}_4^+$  and 0.2% is  $\text{NO}_3^-$ , given the significantly higher  $\text{NH}_4^+$  concentrations in permafrost than  $\text{NO}_3^-$  (Hansen & Elberling, 2023; Marushchak et al., 2021) and allocated these proportions to the soil  $\text{NH}_4^+$  and  $\text{NO}_3^-$  pools accordingly.

## 2.2. Model Calibration and Validation

We used 520 observations at 47 natural ecosystem sites from the northern high latitudes in this study. The observations were obtained through requests from authors or digitized from figures in cited publications. To facilitate meaningful comparisons, all these observations were aggregated into monthly emission data.  $\text{N}_2\text{O}$  flux measurements taken over 5 months or more were selected for model calibration, while measurements from shorter campaigns were used for model validation. We conducted model calibration using 338 (out of 520) observations from 24 sites across the northern high latitudes, including 6 wet tundra (WT)/peatland sites, 6 alpine tundra/dry tundra sites, and 12 boreal forest sites (Table S1 in Supporting Information S1, Figure 2). Model validation was performed with the remaining 182 out of 520 observations from different locations or time periods, including 10 alpine tundra/dry tundra sites, 7 WT/peatland sites, and 6 boreal forest sites (Table S1 in Supporting Information S1, Figure 2).

Data of soil density and pH were obtained from the same publications or relevant publications associated with the same site, or from the global soil bulk density map (GLOBAL SOIL DATA TASK, 2000) and Global Database of Soil Properties (Carter & Scholes, 2000). Meteorological data used as the model forcing, including monthly air temperature, water vapor pressure, precipitation, and cloudiness, were collected from the literature or the Climate Research Unit (CRU TS v. 4.05) (Harris et al., 2020).

We used PEST (V17.2 for Linux) for calibration (<https://pesthhomepage.org/>) of optimal nitrification and denitrification parameters for major natural ecosystem types in the region (Table 1). Calibration for each site was conducted individually and each site was given the same weight. The parameters were obtained through iterative optimization method based on the Gauss-Marquardt-Levenberg (GML) gradient search algorithm, where the parameters were adjusted to minimize the sum of squared weighted residuals between the simulated and observed  $\text{N}_2\text{O}$  emissions at each site. Some observations were measured on an hourly basis and included sporadic high-emission events that were not sustained over a full month. Aggregating these hourly measurements into monthly data could therefore overestimate monthly emissions. We assign less weight to these high-emission events in the calibration process to minimize this but still display the raw observation data in comparison (Figure 3a).

## 2.3. Regional Extrapolation

To obtain spatiotemporally explicit estimations of  $\text{N}_2\text{O}$  emissions at the regional scale, we used the data of land cover, soils, and climate from various sources at a spatial resolution of  $0.5^\circ \times 0.5^\circ$  to drive TEM. We used monthly climate forcing data including those derived from CRU TS v. 4.05 data (Harris et al., 2020) during 1969–2019. Data on soil density and pH were obtained from the global soil bulk density map (GLOBAL SOIL DATA TASK, 2000) and the Global Database of Soil Properties (Carter & Scholes, 2000). The permafrost region with coverage greater than 0%, as estimated by Obu (2021), and the northern permafrost region soil carbon and nitrogen horizontal and vertical distribution dataset from Palmtag et al. (2022) were used. These data were resampled to a  $0.5^\circ \times 0.5^\circ$  resolution for simulations under the permafrost thawing scenario. N deposition effects were simulated during 1984–2016. The regional N deposition data from 1984 to 1986, 1994 to 1996, 2004 to

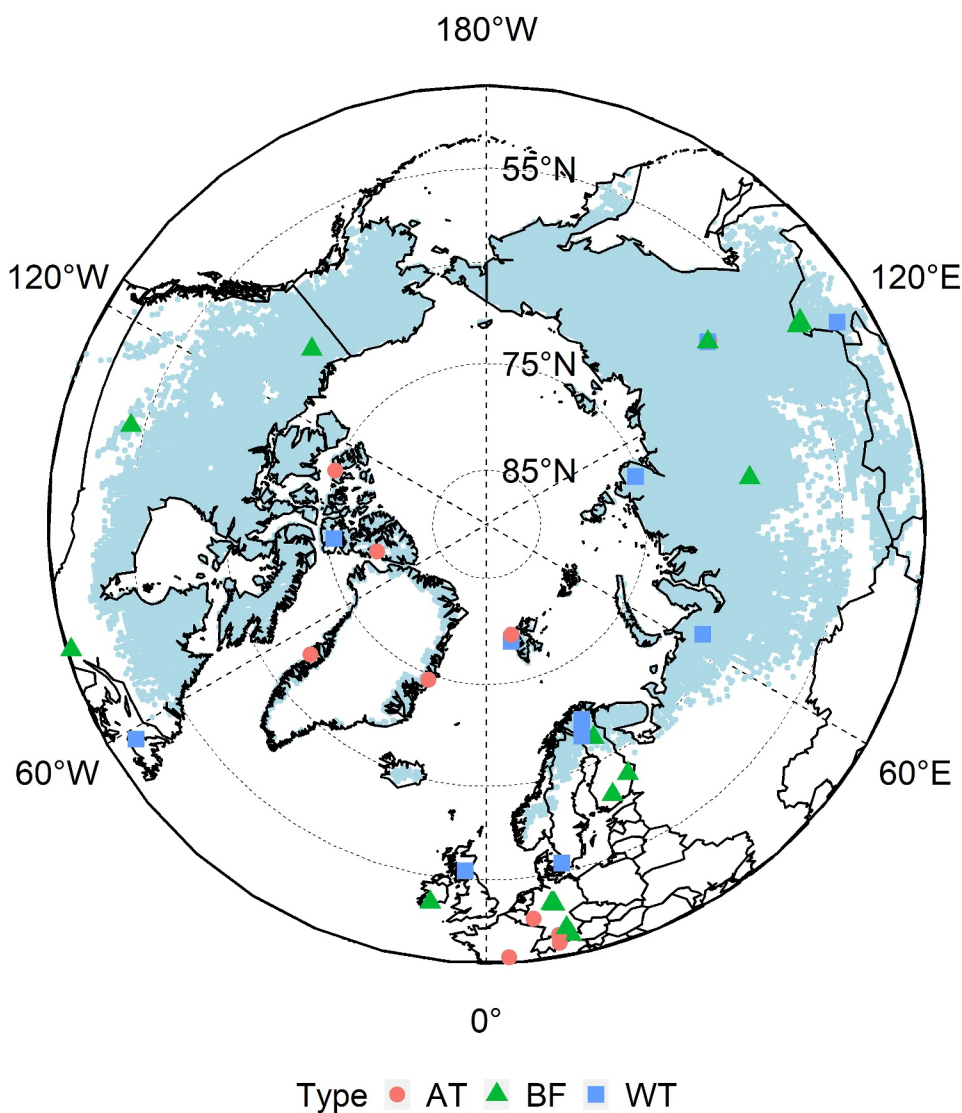


**Figure 2.** Locations of observation sites used in this study. Four alpine tundra sites on the Tibetan Plateau, located south of 45°N, are not shown on this map. The blue area represents the permafrost region with more than 0% coverage, as estimated by Obu (2021), and is used in this study.

**Table 1**  
Statistics of Calibrated Parameter Values in N<sub>2</sub>O Emission Processes Used in This Study, Including the Mean ± Standard Error, Median, and Q1-Q3 Quartiles<sup>a</sup>

		$k_1$	$k_{max}$	$f_{no3k}$	$f_{co2k}$	$k_n$
Boreal Forest	Mean ± SE	0.21 ± 0.05	0.22 ± 0.08	1.24 ± 0.1	0.08 ± 0.01	0.016 ± 0.001
	Median [Q1, Q3]	0.2 [0.13, 0.31]	0.1 [0.04, 0.26]	1.15 [1.15, 1.15]	0.1 [0.09, 0.1]	0.02 [0.01, 0.02]
Wet Tundra	Mean ± SE	0.13 ± 0.08	0.003 ± 0.002	0.6 ± 0.23	0.067 ± 0.02	0.007 ± 0.004
	Median [Q1, Q3]	0.06 [0.00001, 0.16]	0.00001 [0.00001, 0.0009]	0.56 [0.14, 0.95]	0.1 [0.03, 0.1]	0.0007 [0.0006, 0.015]
Alpine Tundra	Mean ± SE	0.24 ± 0.07	0.13 ± 0.07	0.93 ± 0.15	0.08 ± 0.017	0.012 ± 0.004
	Median [Q1, Q3]	0.22 [0.18, 0.29]	0.1 [0.03, 0.11]	1.15 [0.64, 1.15]	0.1 [0.1, 0.1]	0.016 [0.004, 0.02]

<sup>a</sup>Mean values were applied in the base, permafrost thawing, and deposition scenarios. Mean ± SE was used to quantify the model uncertainty (the lower and upper bounds). Detailed parameter definitions and calibration methodologies were provided in the 2.3 Model description.

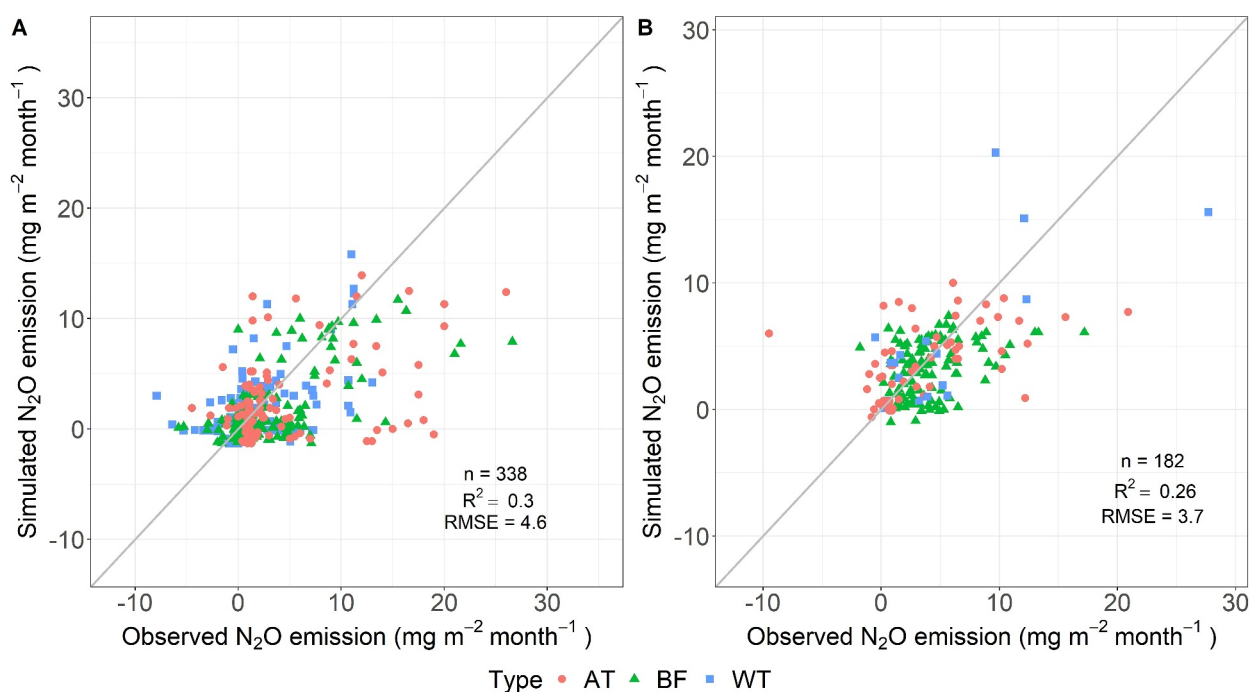


**Figure 3.** Comparison between the simulated and observed  $\text{N}_2\text{O}$  emissions of calibration (a) and validation using the mean value of parameters (b) for alpine tundra (AT), boreal forest (BF) and wet tundra without permafrost thawing effects. The gray line represents  $y = x$ . The observations used for calibration (a) are independent of those used for validation (b).

2006, and 2014 to 2016 was sourced from re-gridded model results from GEOS-Chem (Ackerman et al., 2018), with gaps between modeled years were filled with the average values between two adjacent time periods. We assumed that half of the inorganic N deposition is  $\text{NH}_4^+$ . We used the first-year climate data for model spin-up for at least 50 years to achieve a steady state for the state and flux variables for each grid cell. The regional extrapolation was conducted under three scenarios: base, permafrost thawing, and deposition. In the base scenario, parameter values were set to the mean, mean + SE, mean—SE, median, Q1, and Q3. Since simulations using the mean and median values closely align throughout the period (Figure S1 in Supporting Information S1), only mean values were used in the permafrost thawing and deposition scenarios.

#### 2.4. Model Uncertainty and Sensitivity Analyses

All parameters calibrated in this study (Table 1, Equations 4–7) were positively correlated with nitrification, denitrification and  $\text{N}_2\text{O}$  emission. Therefore, the lower and upper bounds of parameter values (mean—SE and mean + SE) will result in the minimum and maximum estimations of  $\text{N}_2\text{O}$  fluxes. The differences between the maximum and minimum estimations were used as the range of parameter-driven uncertainty in regional nitrification, denitrification and  $\text{N}_2\text{O}$  emissions.

The forcing uncertainties were evaluated with the variation in  $\text{N}_2\text{O}$  emissions, nitrification, and denitrification by changing  $\pm 3^\circ\text{C}$  temperature or  $\pm 30\%$  precipitation in regional simulations. All other meteorological inputs remained constant from 1969 to 2019. Mean parameter values were used for the sensitivity analyses.

#### 2.5. Statistical Analysis

To assess the significance of differences in annual  $\text{N}_2\text{O}$  emissions between the baseline and permafrost thawing simulations, we performed both linear regression and Mann-Kendall tests. A one-way analysis of variance was conducted to evaluate differences in  $\text{N}_2\text{O}$  emission rates among vegetation types, followed by Tukey's honest significant difference test for post hoc comparisons. A *t*-test was also performed to compare the base simulation with the nitrogen deposition simulation. Statistical analyses were conducted using R version 4.3.3 (R Core Team, 2024). The “trend” package was used for Mann-Kendall tests, while the “stats” package was employed for general statistical analyses.

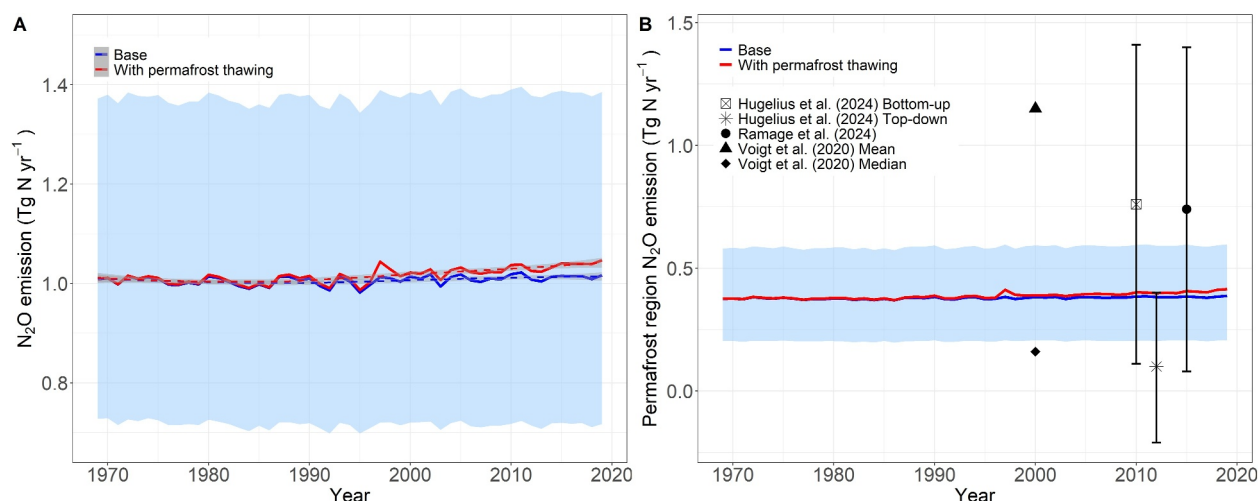


**Figure 4.** Panel A shows annual net N<sub>2</sub>O emissions from natural terrestrial ecosystems in the northern high latitudes from 1969 to 2019. Panel B shows net annual N<sub>2</sub>O emissions from permafrost regions within the northern high latitudes. For both panels, the blue line represents the annual mean emissions of the base simulation (without considering permafrost thawing effects). The red line represents the annual mean emissions considering permafrost thawing effects. Dashed curves are locally estimated scatterplot smoothing (LOOSE) lines for the base simulation and “with permafrost thawing” simulation, respectively. Gray bands around the dashed curves represent 95% confidence intervals of annual emissions for the study period. Black solid dots in panel B represent N<sub>2</sub>O emission estimates from the literature, with values estimated for the permafrost area used in this study for direct comparisons. The light blue shading area represents the lower and upper bounds of the regional N<sub>2</sub>O emissions simulated with lower and upper bounds of parameter values.

### 3. Results

#### 3.1. Annual N<sub>2</sub>O Production, Emissions, and Uptake From the Northern High Latitudes

Terrestrial Ecosystem Model estimated that the annual net N<sub>2</sub>O emissions (production—emission) from natural terrestrial ecosystems in the northern high latitudes (north of 45°N) slightly increased from 1969 to 2019, with the highest value of 1.02 (0.72–1.39) Tg N yr<sup>-1</sup> in 2011 and the lowest value of 0.98 (0.7–1.34) Tg N yr<sup>-1</sup> in 1995, without considering the effect of permafrost thawing (hereafter, referred to as the base simulation). When permafrost thawing effects were included (hereafter, referred to as the permafrost thawing simulation), the emissions were highest in 2019 (1.05 Tg N yr<sup>-1</sup>) and the lowest in 1995 (0.98 Tg N yr<sup>-1</sup>) (Figure 4a). In northern high latitudes, the net N<sub>2</sub>O emission from permafrost thawing simulation is significantly higher than that from the base simulation ( $p < 0.001$ ) and the difference between the base simulation and permafrost thawing simulation increased with time, with the largest difference in 1997, 2018, and 2019 (0.03 Tg N yr<sup>-1</sup>, 3%).

Our calibration provides lower and upper bounds of parameters for each ecosystem type in the northern high latitudes (Table 1). Based on these parameter values, our model estimated that uncertainties of regional N<sub>2</sub>O emissions increased from 0.7 to 0.73 Tg N yr<sup>-1</sup> (lower bound, parameters set mean—SE) and from 1.34 to 1.4 Tg N yr<sup>-1</sup> (upper bound, parameters set mean + SE) for the periods of 1969–2019 (Figure 4a). The upper and lower bounds of annual regional nitrification, denitrification, and N<sub>2</sub>O emission, compared to the base simulation, are summarized in Table 2.

The estimated total N<sub>2</sub>O production showed a slight increase from 1969 to 2019. In the base scenario, the lowest value was observed in 1995 (1.12 Tg N yr<sup>-1</sup>), while the highest value was observed in 2015 (1.15 Tg N yr<sup>-1</sup>). When accounting for permafrost thawing, the peak value reached 1.18 Tg N yr<sup>-1</sup> in 2019.

Total N<sub>2</sub>O uptake in northern high latitudes slightly declined in both base and permafrost thawing simulations, but with small variations from year to year at 0.12 Tg N yr<sup>-1</sup> in base and permafrost thawing simulations (Figure S2B in Supporting Information S1). The upper bound was 0.15 Tg N yr<sup>-1</sup> and the lower bound was 0.1 Tg N yr<sup>-1</sup>. N<sub>2</sub>O uptake accounts for 10.3%–11.1% of the total production and 11.7%–12.6% of the total emission in the base simulation, 10%–11% of total production and 11.3%–12.5% of the total emission in the permafrost thawing simulation.

**Table 2**

*Absolute and Percentage Differences of Parameter-Driven Uncertainties of Annual N<sub>2</sub>O Emissions, Nitrification Rates, and Denitrification Rates Across the Northern High Latitudes and Permafrost Regions Relative to Baseline Conditions*

		Nitrification rate		Denitrification rate		N <sub>2</sub> O emissions	
		(Tg)	(%)	(Tg)	(%)	(Tg)	(%)
Northern high latitudes	Upper bound	3.37 ± 0.11	7.93 ± 0.33	0.47 ± 0.01	18.27 ± 0.42	0.37 ± 0.003	36.57 ± 0.26
	Lower bound	-5.25 ± 0.08	-12.5 ± 0.13	-0.37 ± 0.01	-14.02 ± 0.57	-0.29 ± 0.01	-28.81 ± 0.42
Permafrost region	Upper bound	2.29 ± 0.03	17.32 ± 0.31	0.3 ± 0.01	41.61 ± 0.55	0.21 ± 0.002	54.98 ± 0.38
	Lower bound	-2.72 ± 0.05	-20.55 ± 0.16	-0.25 ± 0.01	-35.2 ± 0.62	-0.18 ± 0.002	-46.28 ± 0.3

*Note.* Results are derived from 51-year simulations (1969–2019), expressed as mean ± standard deviation (SD).

### 3.2. Annual N<sub>2</sub>O Production and Emissions in Permafrost and Non-Permafrost Regions

We estimated permafrost areas are  $19.95 \times 10^6$  km<sup>2</sup> in this region based on Obu (2021) and Palmtag et al. (2022). The net N<sub>2</sub>O emissions from these areas ranged from 0.37 (0.2–0.57) to 0.39 (0.21–0.6) Tg N yr<sup>-1</sup> from 1969 to 2019 in the base simulation. Under permafrost thawing, the net N<sub>2</sub>O emission ranged from 0.37 to 0.41 Tg N yr<sup>-1</sup> (Figure 4b). In the permafrost region, the net N<sub>2</sub>O emission from the permafrost thawing simulation is significantly higher than that from the base simulation ( $p < 0.001$ ) and the difference in total N<sub>2</sub>O emissions between the base and permafrost thawing scenarios increased over time, reaching a maximum difference of over 0.02 Tg N yr<sup>-1</sup> (more than 5%) in 1997 and from 2015 to 2019. In non-permafrost regions, the total N<sub>2</sub>O emissions remained more stable over time, ranging from 0.61 to 0.64 Tg N yr<sup>-1</sup> across both the base and permafrost thawing simulations (Figure S3 in Supporting Information S1).

Similar to the annual net N<sub>2</sub>O emissions (N<sub>2</sub>O production—N<sub>2</sub>O uptake), the N<sub>2</sub>O production from permafrost regions generally increased from 1969 to 2019 (Figure 7d), with the highest value of 0.46 Tg N yr<sup>-1</sup> in 2019 and the lowest value of 0.44 Tg N yr<sup>-1</sup> in 1986 in the base simulation, and the highest in 2019 (0.48 Tg N yr<sup>-1</sup>) and lowest in 1986 (0.44 Tg N yr<sup>-1</sup>) in the permafrost thawing simulation. The difference in N<sub>2</sub>O production in permafrost regions between the base simulation and permafrost thawing simulation increased from 1969 to 2019, with the largest difference in 2015–2019 (>5%).

In permafrost regions, the average annual N<sub>2</sub>O emission in our simulation from boreal forest, dry tundra and WT are significantly different from each other ( $P < 0.001$ ). Under permafrost thawing conditions, tundra ecosystems have higher N<sub>2</sub>O emissions than boreal forest in this region (Table 3, Figure S4 in Supporting Information S1).

### 3.3. Spatial Variability of N<sub>2</sub>O Emissions

For each of the base and the permafrost-thawing simulations, two 5-year time slices (1969–1973 and 2015 to 2019) were taken for the spatial pattern analysis. Spatially, in the base simulation, the N<sub>2</sub>O emissions ranged from -12.47 to 555.25 mg N m<sup>-2</sup> yr<sup>-1</sup> in 1969–1973 and from -12.34 to 555.35 mg N m<sup>-2</sup> yr<sup>-1</sup> in 2015–2019. The ecosystems with net sinks of N<sub>2</sub>O (net emissions <0.0) were mainly scattered in higher latitude regions (>65°N), while the hotspots for net N<sub>2</sub>O sources were concentrated in the lower latitude regions (<65°N) (Figures 5a and 5b). The overall spatial pattern of net N<sub>2</sub>O emission remained relatively stable from 1969 to 2019 (Figures 5a and 5b). However, over this period, changes varied by latitude. Higher latitude grids generally showed an increase in

**Table 3**

*Simulated Annual N<sub>2</sub>O Emissions Across Boreal Forest, Dry Tundra, and Wet Tundra Grids in Permafrost Regions Under Thawing Scenarios From 1969 to 2019*

	Boreal forest (mg N m <sup>-2</sup> yr <sup>-1</sup> )	Dry tundra (mg N m <sup>-2</sup> yr <sup>-1</sup> )	Wet tundra (mg N m <sup>-2</sup> yr <sup>-1</sup> )
Median [Q1, Q3]	12.17 [8.21, 14.9]	18.86 [10.34, 20.46]	15.21 [5.17, 24.33]
Mean ± SD	11.44 ± 6.29	19.92 ± 18.98	15.93 ± 16.17

*Note.* Results are presented as grid-level statistics (mean ± standard deviation, median, and Q1–Q3 quartiles) reflecting spatial variability in emissions.

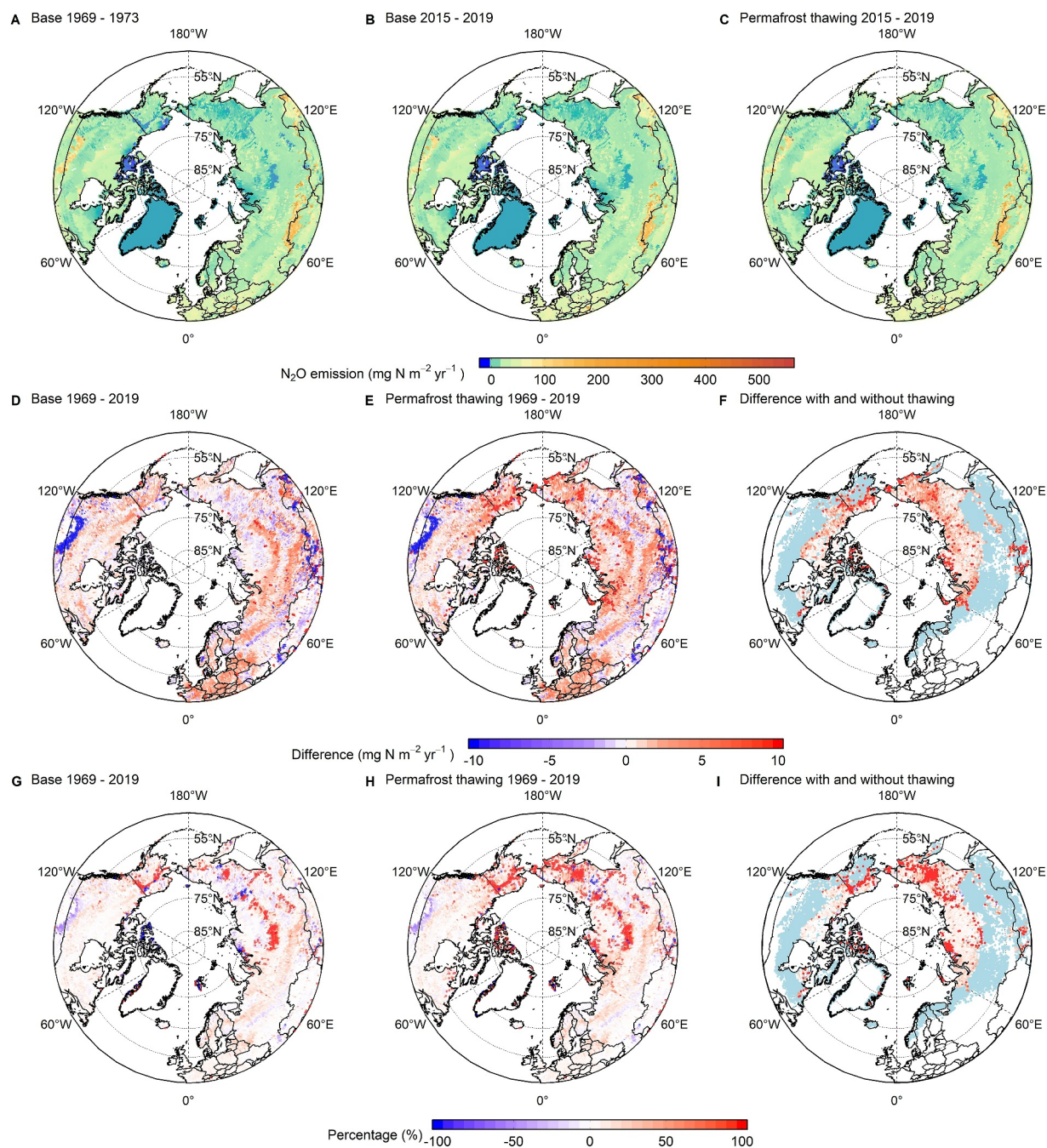


**Figure 5.** Averaged net annual  $N_2O$  emissions in the northern high latitudes from 1969 to 2019: (a) Shows the baseline emissions from 1969 to 1973, (b) presents the baseline emissions from 2015 to 2019, and (c) displays the emissions from 2015 to 2019 considering permafrost thawing effects. In each map, blue areas indicate net  $N_2O$  sinks (negative values). Panels (d–f) illustrate the absolute differences: (d) Is the difference between (a, b, and c) shows the difference between 1969–1973 and 2015–2019 under permafrost thawing effects, and (f) represents the difference between (b, c). Panels (g–i) correspond to the percentage differences related to (d–f), respectively.

emissions, while lower latitude areas in this region exhibited a slight decrease (Figure 5g). The extent of net sink areas of  $N_2O$  reduced from 3.29% to 2.58% over the natural terrestrial ecosystems in the region.

Considering permafrost thawing effects, simulated  $N_2O$  emission ranged from  $-12.47$  to  $554.25\ mg\ N\ m^{-2}\ yr^{-1}$  in 1969–1973 and from  $-10.59$  to  $946.69\ mg\ N\ m^{-2}\ yr^{-1}$  in 2015–2019. Similar to the base simulation, the general spatial pattern did not have an obvious change from 1969 to 2019 (Figures 5a and 5c). However, compared with the

**Table 4**  
*Sensitivity of Annual N<sub>2</sub>O Emissions, Nitrification Rates, and Denitrification Rates to Temperature and Precipitation Changes in the Northern High Latitudes Between 1969 and 2019, Relative to Baseline Simulations*

	Temperature +3°C	Temperature -3°C	Precipitation +30%	Precipitation -30%
N <sub>2</sub> O emissions (%)	20.6 ± 0.53	-19.6 ± 0.44	3.4 ± 0.49	-2.3 ± 0.7
Nitrification rate (%)	8.5 ± 0.34	-16.0 ± 0.27	0.3 ± 0.2	-1.6 ± 0.28
Denitrification rate (%)	23.8 ± 0.69	-21.3 ± 0.48	1.6 ± 0.54	0.2 ± 0.63

*Note.* Results are expressed as mean ± standard deviation (SD), derived from 51-year average simulations spanning the study period. Parameter uncertainties were excluded to isolate the direct impacts of climatic drivers on ecosystem nitrogen dynamics.

base simulation, there are many areas having increased emissions from 1969 to 2019, particularly in the higher latitudes (Figures 5e and 5h), with permafrost coverage greater than 90% in Obu (2021). The proportion of grid cells acting as net sink of N<sub>2</sub>O decreased from 3.29% to 2.38%.

Although the total N<sub>2</sub>O emissions from northern high latitudes, including permafrost regions, increase only slightly compared with base simulations, the spatial variation of emissions is substantial, ranging from 0 to 925 mg N m<sup>-2</sup> yr<sup>-1</sup>. Some grids show changes greater than 10 mg N m<sup>-2</sup> yr<sup>-1</sup> and more than 100% compared with the base simulation in 2015–2019 (Figures 5f and 5i). The mean N<sub>2</sub>O emission increase compared with base simulation is 3.35 mg N m<sup>-2</sup> yr<sup>-1</sup>, with a median of 0.97 mg N m<sup>-2</sup> yr<sup>-1</sup>. Overall, permafrost thawing significantly elevates the regional N<sub>2</sub>O emissions.

### 3.4. Model Sensitivity

Model sensitivity analysis shows that N<sub>2</sub>O emissions are highly sensitive to changes in temperature (±3°C) but less sensitive to precipitation change (±30%). In general, higher temperature and precipitation levels enhance N<sub>2</sub>O emissions in the region, while lower temperature and precipitation inhibit the emission. The regional nitrification rate increased by 8.5%, while denitrification increased by 23% under 3°C temperature increase, leading to an N<sub>2</sub>O emission increase of 21% (Table 4). Conversely, decreasing temperature by 3°C resulted in a similar magnitude decrease in N<sub>2</sub>O emissions and nitrification rate, but denitrification tended to decrease more. The total nitrification and denitrification rates in the northern high latitudes exhibited smaller sensitivity to precipitation. Precipitation changes by 30% did not induce dramatic changes in both the nitrification rate and denitrification rate; thus, the regional net N<sub>2</sub>O emissions. This is primarily due to our method that evenly assigns monthly precipitation data to each day within the month; the low daily precipitation did not yield substantial changes in daily soil moisture despite a 30% variation in monthly precipitation. Consequently, both nitrification and denitrification rates did not experience substantial shifts. However, different sites displayed varying responses. Spatially, there were various responses to the changes in precipitation in nitrification and denitrification rates (Figure S8, S9 in Supporting Information S1). Nitrification exhibits a non-linear optimal response to soil moisture; thus, soil moisture differences in the region result in substantial differences in nitrification rates under both higher (+30%) and lower (-30%) precipitation conditions compared with their initial soil moisture conditions. In addition to the effect of precipitation on soil moisture, the denitrification rate is also influenced by the nitrification rate since nitrification provides substrate NO<sub>3</sub><sup>-</sup> for denitrifiers; thus, even when soil moisture conditions become more conducive to denitrification, the denitrification rate may not experience a significant increase, which leads to variation in the denitrification rate in different grid cells in the region.

## 4. Discussion

### 4.1. Comparison With Other Studies

Global N<sub>2</sub>O emissions from natural sources have been estimated to range from 8 to 12.5 Tg N yr<sup>-1</sup> in recent decades (Syakila and Kroeze., 2011; Bouwman et al., 2013; Yu & Zhuang, 2019; Tian et al., 2020), while the specific estimates for net N<sub>2</sub>O emissions from the northern high latitudes have been lacking thus far. From site-level studies, the median and Q1, Q3 growing season N<sub>2</sub>O emissions range from 19 to 60 [-9, 481] μg N<sub>2</sub>O-N m<sup>-2</sup> day<sup>-1</sup> in all vegetated permafrost landscapes including peatlands, uplands, wetlands (Voigt et al., 2020), which aligns with the range of our simulation. A modeling analysis for the high Arctic showed an increase in N<sub>2</sub>O

emissions after permafrost thawing with an average value of  $2 \text{ mg N m}^{-2} \text{ yr}^{-1}$  (Lacroix et al., 2022), consistent with our simulation.

Voigt et al. (2020) estimated that the annual  $\text{N}_2\text{O}$  budget of northern hemisphere regions ( $17.8 \times 10^6 \text{ km}^2$ ) is  $0.07\text{--}0.51$  (median-mean)  $\text{Tg N yr}^{-1}$  over a 100-day growing season, and  $0.14$  to  $1.03$  (median-mean)  $\text{Tg N yr}^{-1}$  by upscaling from experimental flux studies in the growing season. In a new study (Hugelius et al., 2024), bottom-up and top-down approaches show that estimates of  $\text{N}_2\text{O}$  from  $18.42 \times 10^6 \text{ km}^2$  northern permafrost regions are  $0.7$  ( $0.1, 1.3$ ) and  $0.09$  ( $-0.19, 0.37$ )  $\text{Tg N yr}^{-1}$ , respectively. Ramage et al. (2024) projected that the  $\text{N}_2\text{O}$  emissions from the northern permafrost region ( $18.5 \times 10^6 \text{ km}^2$ ) ranged from  $0.07\text{--}1.3 \text{ Tg N yr}^{-1}$ . For the same area, the simulated  $\text{N}_2\text{O}$  emissions from Voigt et al. (2020), Hugelius et al. (2024) and Ramage et al. (2024) are  $0.16\text{--}1.15$  (median-mean)  $\text{Tg N yr}^{-1}$ ,  $0.11$  to  $1.41$  (bottom-up) and  $-0.21$  to  $0.4 \text{ Tg N yr}^{-1}$  (top-down),  $0.08$  to  $1.4 \text{ Tg N yr}^{-1}$ , respectively. Our estimated  $\text{N}_2\text{O}$  emission from the permafrost region falls within these ranges (Figure 4b).

In our simulation,  $\text{N}_2\text{O}$  uptake primarily occurs during winter, when soils exhibit the lowest  $\text{N}_2\text{O}$  production, with maximum uptake rates reaching  $0.05 \text{ mg N m}^{-2} \text{ day}^{-1}$ . Among the observational studies we have examined, seven studies, including those by Butterbach-Bahl et al., Dinsmore et al. (2017), Glatzel and Stahr. (2001), Lohila et al. (2010), Jørgensen and Elberling (2012), Cantarel et al. (2011), and Drewer et al. (2010), report negative  $\text{N}_2\text{O}$  fluxes in winter. The observed winter  $\text{N}_2\text{O}$  uptake rates across these studies ranged from  $0.014$  to  $0.36 \text{ mg N m}^{-2} \text{ day}^{-1}$ . Siljanen et al. (2020) reported that  $\text{N}_2\text{O}$  uptake in boreal forest soils can reach up to  $0.4 \text{ mg N m}^{-2} \text{ day}^{-1}$ . The highest uptake occurred during the low-temperature seasons, which aligns with our estimates. A previous study suggests that the median uptake potential is  $4 \mu\text{g N m}^{-2} \text{ h}^{-1}$  and the total global consumption is less than  $0.3 \text{ Tg N yr}^{-1}$  (Schlesinger, 2013). The projected sink is about 5% of the currently estimated global net  $\text{N}_2\text{O}$  fluxes from soils to the atmosphere (Schlesinger, 2013), which is lower than our estimates in the northern high latitudes.

Stable isotope analysis has indicated that in soils with a water-filled pore space of 50%–55%, nitrification is the dominant (>80%) process contributing to  $\text{N}_2\text{O}$  emissions (Ma et al., 2007). Conversely, in soils with a water-filled pore space ranging from 60% to 70%, high  $\text{N}_2\text{O}$  emissions are linked to denitrification (Gil et al., 2017; Marshchak et al., 2011; Voigt et al., 2020). Our simulations suggest that nitrification is more widespread than denitrification in the northern high latitudes. However, denitrification remains the primary source of  $\text{N}_2\text{O}$  emissions throughout the entire northern high latitudes (Figures 6g and 6h).

#### 4.2. The Role of Permafrost Thawing

Permafrost thawing releases more soil organic N for mineralization as well as the inorganic N for nitrification and denitrification. Consequently, increasing the amount of inorganic N availability resulted in higher nitrification and denitrification rates (Figures 6a, 6b, 6c).

In the base and permafrost thawing simulations, the regional nitrification rate, denitrification rate, production of  $\text{N}_2\text{O}$  resulting from nitrification, and production of  $\text{N}_2\text{O}$  resulting from denitrification showed upward trends from 1969 to 2019 (Figures 6e, 6f, 6g, 6h). The higher  $\text{N}_2\text{O}$  production from both nitrification and denitrification contributes to an overall increase in total  $\text{N}_2\text{O}$  production. The pulse in denitrification,  $\text{N}_2\text{O}$  production and net  $\text{N}_2\text{O}$  emission is associated with the pulse of high nitrogen input driven by the extensive permafrost thawing depth increase (Figures 6a and 6b).

The averaged maximum permafrost thawing depth in the northern high latitude permafrost region increased by  $0.5 \text{ m}$  in our simulation (Figure S5B in Supporting Information S1), meaning that the organic nitrogen and carbon stored in the  $0.5 \text{ m}$  thawed layer were made available for decomposition. Average temperature in the northern high latitude permafrost region increases from  $-8.8^\circ\text{C}$  to  $-6.4^\circ\text{C}$  during 1969–2019 according to CRU Ts v. 4.05. The increasing thawing depth from 1969 to 2019 is small in the current simulation. However, the Arctic region is predicted to warm up to  $3\text{--}7^\circ\text{C}$  and the top  $3 \text{ m}$  permafrost is expected to degrade (Schuur and Abbott., 2011) for 47%–61% area by 2100 under a high warming scenario, which will likely significantly intensify  $\text{N}_2\text{O}$  emissions from the region.

#### 4.3. The Role of N Deposition in Regional $\text{N}_2\text{O}$ Emissions

In field observations, nitrogen deposition has been shown to induce a substantial increase in  $\text{N}_2\text{O}$  emissions by 95% in dry alpine meadows (Yan et al., 2018), grasslands (Du et al., 2021), and boreal and temporal forests

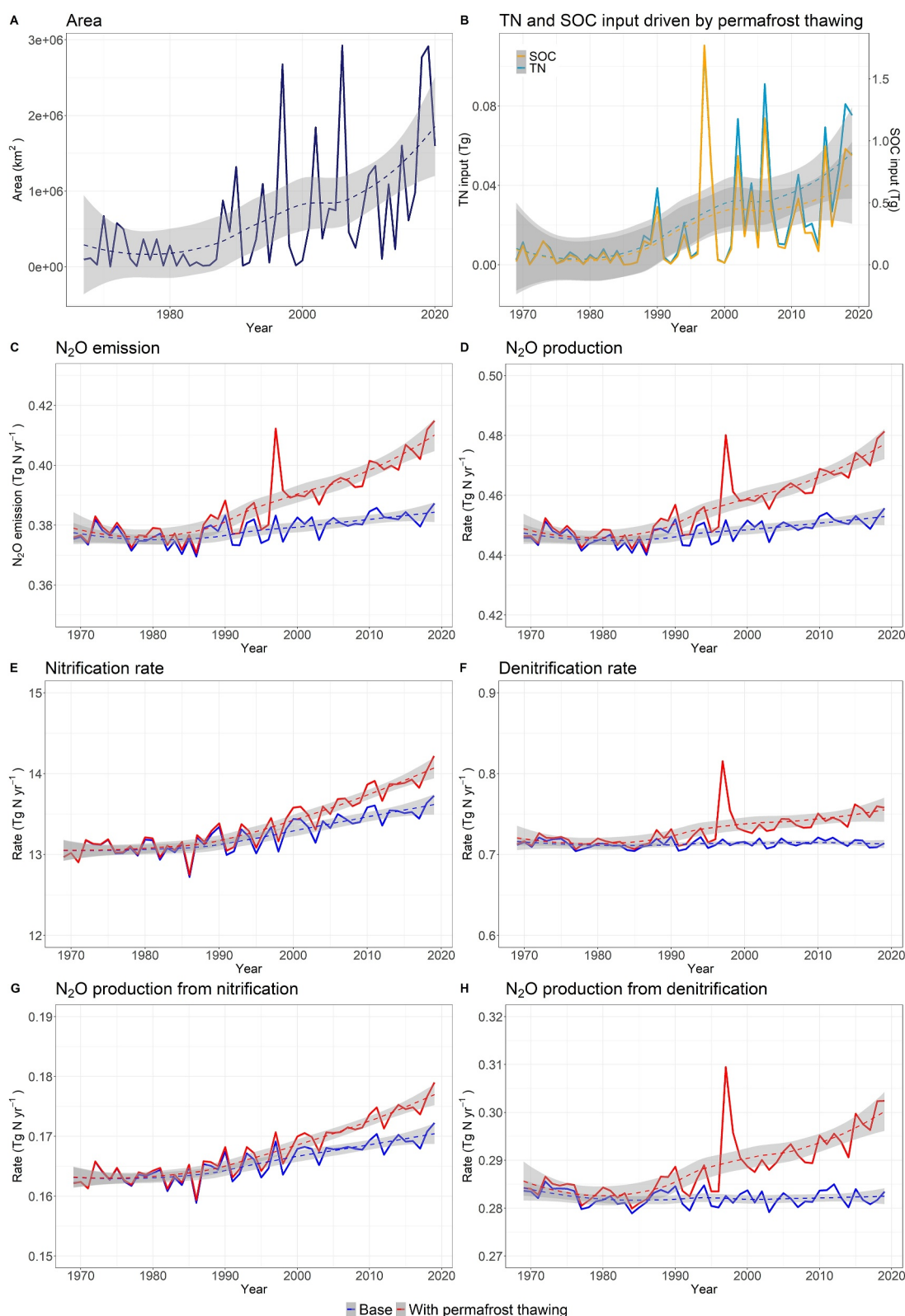


**Figure 6.** Simulated area experiencing the increase of maximum active layer depth in permafrost region(a), SOC and TN input (b), total N<sub>2</sub>O emission (c), total N<sub>2</sub>O production (d), nitrification rate (e), denitrification rate (f), N<sub>2</sub>O production from nitrification(g) and N<sub>2</sub>O production from denitrification (h) in the base (blue) and permafrost thawing simulations (red), respectively, from 1969 to 2019. Dashed curves are locally estimated scatterplot smoothing (LOOSE) lines, and the gray bands around the dashed curves are 95% confidence intervals of annual results for the study period.

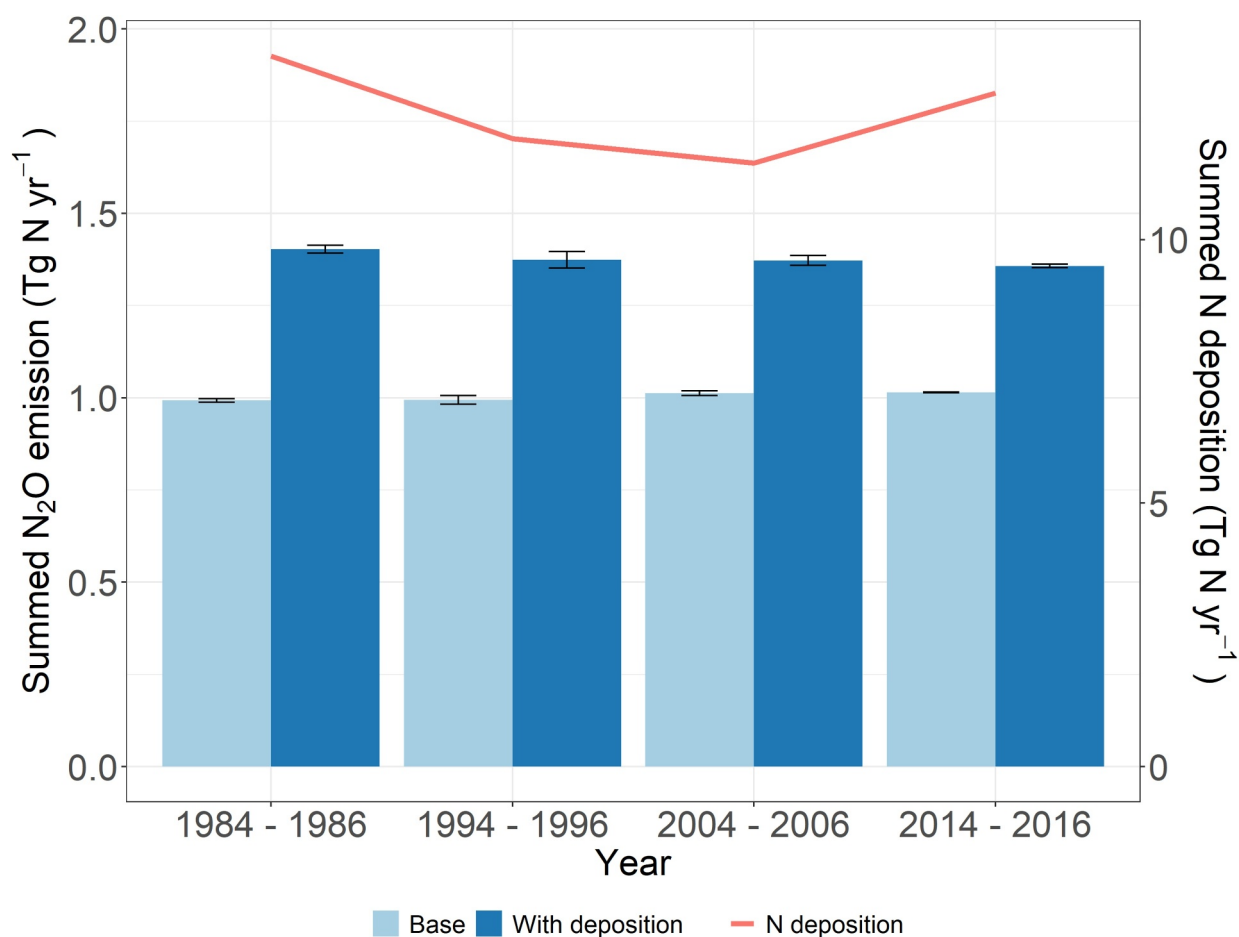


**Figure 7.** Modeled annual net N<sub>2</sub>O emissions (mean ± standard deviation (SD)) from northern high latitudes for the periods 1984–1986, 1994–1996, 2005–2006, and 2014–2016 with and without considering N deposition effects. Error bars represent the SD over each 3-year bin. The red line represents the total N deposition in the northern high latitudes.

(Deng et al., 2020). In our simulation, the impact of N deposition on N<sub>2</sub>O emissions varies spatially depending on the initial N contents and the amount of N deposition.

Our simulation indicates that nitrogen deposition from the atmosphere leads to a significant increase ( $37.2 \pm 2.9\%$ ,  $p < 0.001$ ) in the total N<sub>2</sub>O emissions compared with the simulation without N deposition (Figure 7). With N deposition from the atmosphere, although the spatial distribution of net N<sub>2</sub>O sink and the source remains the same, there are more grid cells in lower latitudes (<60°) that have high N<sub>2</sub>O emissions (>100 mg N m<sup>-2</sup> yr<sup>-1</sup>, Figure 8), generally following the spatial pattern of nitrogen deposition (Ackerman et al., 2018). N<sub>2</sub>O emissions from grids in higher latitudes show a slight increase in absolute values (<10 mg N m<sup>-2</sup> yr<sup>-1</sup>), but with a more than 50% increase compared to simulations without nitrogen deposition (Figures 8c and 8d). This is primarily because these areas, which were previously nitrogen-limited, now benefit from increased nitrogen availability.

The effects of N deposition are greater than the effects of permafrost thawing, primary because the N inputs from N deposition (>10 Tg N yr<sup>-1</sup>, Figure 7) are much greater than the total nitrogen input from permafrost thawing in this region (<0.1 Tg N yr<sup>-1</sup>, Figure 6b).

#### 4.4. Limitations and Future Studies

This study is subject to several limitations that warrant consideration. Primarily, the current calibration and validation rely on observational datasets with limited spatiotemporal coverage, particularly evident in Arctic permafrost regions. While the absolute emission trends remain statistically constrained by current observational

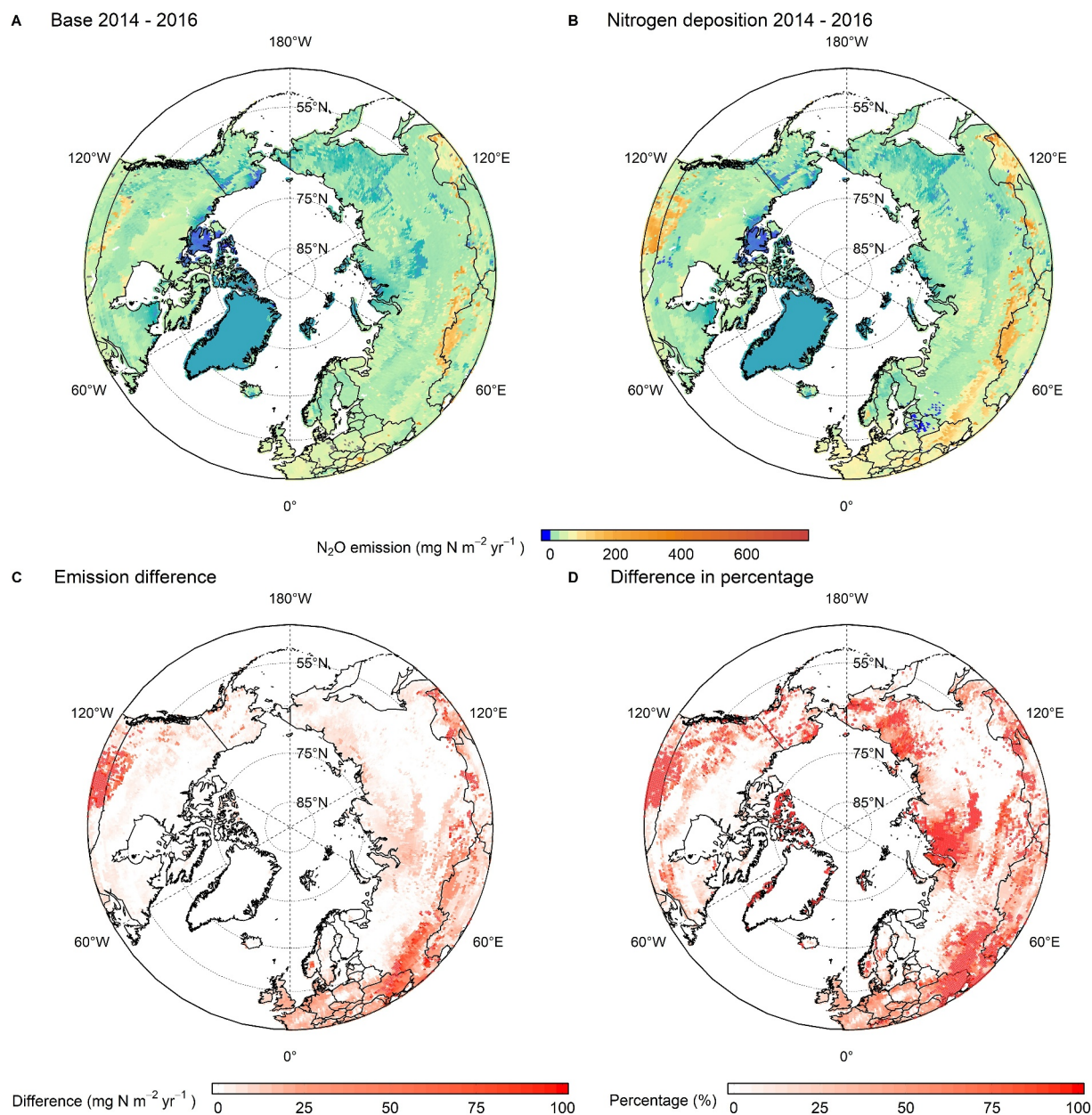


**Figure 8.** Estimated net  $\text{N}_2\text{O}$  emissions from the northern high latitudes from 2014 to 2016 with (b) and without (a) considering N deposition effects. Blue indicates net sink (negative values). The absolute difference in  $\text{N}_2\text{O}$  emissions between A and B is shown in panel (c), while the percentage difference is illustrated in panel (d).

limits, our estimation uncertainty characterization establishes critical priorities for the necessity for expanding observational networks in these areas to better resolve the variability of critical drivers (e.g., soil moisture, temperature, and nitrogen availability) that govern  $\text{N}_2\text{O}$  emissions and advance our mechanistic understanding of the heterogeneous environmental drivers modulating  $\text{N}_2\text{O}$  fluxes across northern permafrost domains. Such improvements would not only refine parameter accuracy and reduce uncertainties in current estimates, but also significantly improve process representation in biogeochemical models, thereby strengthening predictive capabilities under various climate change scenarios.

Second,  $\text{N}_2\text{O}$  uptake is calculated based on the constant  $\text{N}_2\text{O}$  concentration in the atmosphere and the physical process of diffusion in the current model. However, the soil released  $\text{N}_2\text{O}$  increases, leading to higher  $\text{N}_2\text{O}$  concentrations in the atmosphere, consequently, increasing the  $\text{N}_2\text{O}$  uptake from the atmosphere.  $\text{N}_2\text{O}$  is consumed through several reactions of nitrification (Wrage et al., 2004), and under anaerobic

conditions, incomplete denitrification produces  $N_2O$ , whereas the terminal step of denitrification (i.e., the reduction of  $N_2O$  to  $N_2$  with the absence of *nosZ* gene) consumes  $N_2O$  (Shan et al., 2021; Wen et al., 2016). In addition, within the soil profile and in the soil air-filled pores,  $N_2O$  can be further reduced to  $N_2$  during its transport to the soil surface (Chapuis-Lardy et al., 2007; Wen et al., 2016; Yang & Silver, 2016). We expect an increase in  $N_2O$  uptake by taking these processes into account in our future modeling.

Third, high  $N_2O$  emissions during spring thawing and later fall freeze squeezing have been observed. Three studies used for model calibration and validation reported these “shoulder season” emissions (Heinzle et al., 2023; Jørgensen & Elberling, 2012; Merbold et al., 2013). The higher shoulder emission pattern was also simulated in the arctic tundra by Lacroix et al. (2022). Two sources have been proposed to contribute to the enhanced  $N_2O$  emissions upon permafrost thawing, including the seasonal freeze-thaw cycles that physically release  $N_2O$  produced throughout the winter and trapped under frozen surface layers and the emission of newly produced  $N_2O$ . While early studies suggested that the physical release of accumulated  $N_2O$  from subsurface soil layers was the primary mechanism contributing to spring thaw emissions (Risk et al., 2013), most current studies favor the newly produced  $N_2O$  as microorganisms remain active during both periods (Risk et al., 2013; Röver et al., 1998; Teepe, Brumme, et al., 2004) because the timing and amount of  $N_2O$  release during thawing do not correspond to the amount of  $N_2O$  trapped in soils (Furon et al., 2008; Wagner-Riddle et al., 2008). These “shoulder season” emissions have not been well modeled as the model requires considering the snow dynamics and soil physical models need to be driven with daily data to capture these finer temporal scale dynamics. The time step in the current model is not fine enough to account for these freeze-thaw processes. In current modeling, the  $N_2O$  emission mainly happens in the growing season, with  $N_2O$  emission in winter being negligible. This may cause an underestimation of annual  $N_2O$  emissions.

Fourth, while our model simulates nitrogen mineralization and denitrification by taking into account of soil nitrogen availability and environmental factors, recent studies also suggested that soil carbon to nitrogen (C/N) ratio may play a role in influencing nitrification (Bengtsson et al., 2003; Elrys et al., 2021). This ratio affects the abundance of ammonia-oxidizing bacteria and archaea (AOA) (Xiao et al., 2021). Missing this stoichiometric control factor in our model may introduce uncertainties to our estimates.

Fifth, in our simulation, plant N uptake was based on gross primary productivity and soil N concentration. However, the extent to which plants can utilize the newly available N from permafrost thaw is complex and often constrained by factors such as the vertical distribution of N within the soil profile, the timing of N release, and competition with other plants and microorganisms (Lacroix et al., 2022; Pedersen et al., 2020). Permafrost thaw experiments have shown a strong increase in total root length and growth in the active layer, with deep roots extending into the newly thawed permafrost layer beneath (Blume-Werry et al., 2019). This adaptation of Arctic vegetation to deeper thaw depths could limit soil N availability and reduce  $N_2O$  emissions due to the increased N uptake by vegetation, which may bias our simulation.

Sixth, our model was run at a  $0.5^\circ \times 0.5^\circ$  resolution, which covers a large area with significant spatial heterogeneity in landscapes, vegetation types, and soil organic carbon (SOC) and total nitrogen (TN) storage, particularly in the Yedoma permafrost region (Mishra et al., 2021; Strauss et al., 2022). Finer-scale simulations could help reduce the uncertainty in N release through gas or other pathways.

Seventhly, our freeze-thaw modeling estimated the active layer dynamics, which were used to quantify the additional organic and inorganic N for  $N_2O$  production. However, we have not explicitly modeled the effects of permafrost thaw on soil moisture conditions because of the lack of spatially explicit ice content information for the region. Moving forward, we will revise the soil thermal and hydrological components of our modeling framework to incorporate the extra water from thawing permafrost and melting ground ice. This enhancement will allow us to estimate soil moisture more accurately, a critical driver for improving  $N_2O$  emission estimation (Zhuang et al., 2001, 2003).

Lastly, although we have included four vegetated peatlands in the calibration process and four peatlands in validation, and our total estimated  $N_2O$  emission from permafrost regions aligns with other studies, our model does not include a module specifically for simulating peatland  $N_2O$  emissions. Voigt et al. (2020) demonstrated that permafrost peatlands currently represent the highest  $N_2O$  emitters from the Arctic permafrost-affected soils. Northern peatlands are estimated to cover  $3.7 \pm 0.5$  million  $km^2$  and stored  $10 \pm 7$  Pg N. However, they are a

minor source for nitrous oxide, emitting  $0.022 \pm 0.005 \text{ Tg N yr}^{-1}$  (Hugelius et al., 2020),  $0.07 \text{ Tg N yr}^{-1}$  (Zhao & Zhuang, 2024) and  $0.03$  to  $0.1 \text{ Tg N yr}^{-1}$  (Martikainen et al., 1993), which is equivalent to less than 5% of our simulated total  $\text{N}_2\text{O}$  emissions for the entire northern high latitudes. Nonetheless, they represent a larger proportion of permafrost regions in northern high latitudes (10%–30%). Consequently, the absence of an explicit peatland  $\text{N}_2\text{O}$  emission modeling is unlikely to make a significant difference from our current estimates for the northern high latitudes.

## 5. Conclusions

This study advances the quantification of  $\text{N}_2\text{O}$  fluxes in northern high-latitude ecosystems and permafrost regions with a process-based modeling framework that integrates three critical mechanisms: (a) enhancing the representation of physical effects in nitrification and denitrification modeling while incorporating nitrogen loss through gas emissions with empirical equations, (b) accounting for permafrost thaw-induced biogeochemical changes, and (c) incorporating the latest spatially explicit and depth-resolved permafrost C/N stocks, atmospheric  $\text{N}_2\text{O}$  uptake dynamics, and anthropogenic nitrogen deposition effects. Our findings demonstrate that the confluence of climate warming and nitrogen enrichment has transformed these ecosystems into progressively stronger net  $\text{N}_2\text{O}$  sources over the past five decades, with permafrost degradation emerging as a key amplifier of regional emission heterogeneity. While the modeled 5% (over  $0.02 \text{ Tg N yr}^{-1}$ ) emission increase from thawing permafrost may appear modest at the regional scale, localized hotspots exhibit over  $900 \text{ mg N m}^{-2} \text{ yr}^{-1}$  enhancement, underscoring the high spatial variability.

Parameter-driven uncertainties in  $\text{N}_2\text{O}$  emission range from  $-28.81\%$  to  $36.57\%$  ( $-0.29$  to  $0.37 \text{ Tg N yr}^{-1}$ ) for the northern high-latitude region and from  $-46.38\%$  to  $54.98\%$  ( $-0.18$  to  $0.21 \text{ Tg N yr}^{-1}$ ) for the permafrost region, underscoring the need for expanded observational studies to reduce uncertainties. Long-term monitoring beyond the growing season and at finer temporal resolutions is crucial to improving model calibration and reducing uncertainties. Further experimental research on microbial functional processes and nitrogen isotope dynamics will provide valuable insights into nitrogen cycling mechanisms in these climate-sensitive northern high latitude ecosystems. Additionally, incorporating more high-latitude observations and refining soil thermal and hydrology dynamics in freeze-thaw processes, permafrost-plant-microorganism interactions will be essential for advancing our understanding of  $\text{N}_2\text{O}$  fluxes in northern high latitudes.

## Data Availability Statement

The TEM codes, outputs, and samples of the running directory can be accessed via the Purdue University Research Repository Yuan et al. (2023) and Yuan et al. (2025) (<https://purr.purdue.edu/publications/4285/1> and <https://purr.purdue.edu/publications/4285/2>).

## References

- Abbott, B. W., & Jones, J. B. (2015). Permafrost collapse alters soil carbon stocks, respiration,  $\text{CH}_4$ , and  $\text{N}_2\text{O}$  in upland tundra. *Global Change Biology*, 21(12), 4570–4587. <https://doi.org/10.1111/gcb.13069>
- Ackerman, D., Millet, D. B., & Chen, X. (2019). Global estimates of inorganic nitrogen deposition across four decades. *Global Biogeochemical Cycles*, 33(1), 100–107. <https://doi.org/10.1029/2018GB005990>
- Ackerman, D. E., Chen, X., & Millet, D. B. (2018). Global nitrogen deposition ( $2^\circ \times 2.5^\circ$  grid resolution) simulated with GEOS-Chem for 1984–1986, 1994–1996, 2004–2006, and 2014–2016 [Dataset]. *Data Repository for the University of Minnesota*. <https://doi.org/10.13020/D6KX2R>
- Anger, M., Hoffmann, C., & Kühbauch, W. (2003). Nitrous oxide emissions from artificial urine patches applied to different N-fertilized swards and estimated annual  $\text{N}_2\text{O}$  emissions for differently fertilized pastures in an upland location in Germany. *Soil Use & Management*, 19(2), 104–111. <https://doi.org/10.1111/j.1475-2743.2003.tb00288.x>
- Bateman, E. J., & Baggs, E. M. (2005). Contributions of nitrification and denitrification to  $\text{N}_2\text{O}$  emissions from soils at different water-filled pore space. *Biology and Fertility of Soils*, 41(6), 379–388. <https://doi.org/10.1007/s00374-005-0858-3>
- Beermann, F., Langer, M., Wetterich, S., Strauss, J., Boike, J., Fiencke, C., et al. (2017). Permafrost thaw and liberation of inorganic nitrogen in Eastern Siberia. *Permafrost and Periglacial Processes*, 28(4), 605–618. <https://doi.org/10.1002/ppp.1958>
- Bengtsson, G., Bengtson, P., & Månsson, K. F. (2003). Gross nitrogen mineralization-immobilization-and nitrification rates as a function of soil C/N ratio and microbial activity. *Soil Biology and Biochemistry*, 35(1), 143–154. [https://doi.org/10.1016/S0038-0717\(02\)00248-1](https://doi.org/10.1016/S0038-0717(02)00248-1)
- Blume-Werry, G., Milbau, A., Teuber, L. M., Johansson, M., & Dorrepaal, E. (2019). Dwelling in the deep – Strongly increased root growth and rooting depth enhance plant interactions with thawing permafrost soil. *New Phytologist*, 223(3), 1328–1339. <https://doi.org/10.1111/nph.15903>
- Borge, A. F., Westermann, S., Solheim, I., & Etzelmüller, B. (2017). Strong degradation of palsas and peat plateaus in northern Norway during the last 60 years. *The Cryosphere*, 11(1), 1–16. <https://doi.org/10.5194/tc-11-1-2017>
- Bouwman, A. F., Beusen, A. H. W., Griffioen, J., Van Groenigen, J. W., Hefting, M. M., Oenema, O., et al. (2013). Global trends and uncertainties in terrestrial denitrification and  $\text{N}_2\text{O}$  emissions. *Philosophical Transactions of the Royal Society B: Biological Sciences*, 368(1621), 20130112. <https://doi.org/10.1098/rstb.2013.0112>

## Acknowledgments

This research has been supported by the National Science Foundation (Grant 1802832).

- Brown, J., Ferrians, O., Heginbottom, J. A., & Melnikov, E. (2002). Circum-Arctic map of permafrost and ground-ice conditions, version 2 [Dataset]. *National Snow and Ice Data Center*. <https://doi.org/10.7265/skbg-kf16>
- Brummell, M. E., Farrell, R. E., & Siciliano, S. D. (2012). Greenhouse gas soil production and surface fluxes at a high arctic polar oasis. *Soil Biology and Biochemistry*, *52*, 1–12. <https://doi.org/10.1016/j.soilbio.2012.03.019>
- Butterbach-Bahl, K., Gasche, R., Huber, C., Kreuzer, K., & Papen, H. (1998). Impact of N-input by wet deposition on N-trace gas fluxes and CH<sub>4</sub>-oxidation in spruce forest ecosystems of the temperate zone in Europe. *Atmospheric Environment*, *32*(3), 559–564. [https://doi.org/10.1016/S1352-2310\(97\)00234-3](https://doi.org/10.1016/S1352-2310(97)00234-3)
- Cantarel, A. A. M., Bloor, J. M. G., Deltroy, N., & Soussana, J.-F. (2011). Effects of climate change drivers on nitrous oxide fluxes in an upland temperate grassland. *Ecosystems*, *14*(2), 223–233. <https://doi.org/10.1007/s10021-010-9405-7>
- Carter, A. J., & Scholes, R. J. (2000). SoilData v2.0: Generating a global Database of soil Properties CSIR environmentek.
- Chapuis-Lardy, L., Wrage, N., Metay, A., Chotte, J., & Bernoux, M. (2007). Soils, a sink for N<sub>2</sub>O? A review. *Global Change Biology*, *13*(1), 1–17. <https://doi.org/10.1111/j.1365-2486.2006.01280.x>
- Chen, Q., Zhu, R., Wang, Q., & Xu, H. (2014). Methane and nitrous oxide fluxes from four tundra ecotopes in Ny-Ålesund of the High Arctic. *Journal of Environmental Sciences*, *26*(7), 1403–1410. <https://doi.org/10.1016/j.jes.2014.05.005>
- Christiansen, J. R., Gundersen, P., Frederiksen, P., & Vesterdal, L. (2012). Influence of hydromorphic soil conditions on greenhouse gas emissions and soil carbon stocks in a Danish temperate forest. *Forest Ecology and Management*, *284*, 185–195. <https://doi.org/10.1016/j.foreco.2012.07.048>
- Conant, R. T., Ryan, M. G., Ågren, G. I., Birge, H. E., Davidson, E. A., Eliasson, P. E., et al. (2011). Temperature and soil organic matter decomposition rates - Synthesis of current knowledge and a way forward. *Global Change Biology*, *17*(11), 3392–3404. <https://doi.org/10.1111/j.1365-2486.2011.02496.x>
- Cui, Q., Song, C., Wang, X., Shi, F., Yu, X., & Tan, W. (2018). Effects of warming on N<sub>2</sub>O fluxes in a boreal peatland of Permafrost region, Northeast China. *Science of The Total Environment*, *616*–617, 427–434. <https://doi.org/10.1016/j.scitotenv.2017.10.246>
- Dai, Z., Yu, M., Chen, H., Zhao, H., Huang, Y., Su, W., et al. (2020). Elevated temperature shifts soil N cycling from microbial immobilization to enhanced mineralization, nitrification and denitrification across global terrestrial ecosystems. *Global Change Biology*, *26*(9), 5267–5276. <https://doi.org/10.1111/gcb.15211>
- Del Grosso, S. J., Parton, W. J., Mosier, A. R., Ojima, D. S., Kulmala, A. E., & Phongpan, S. (2000). General model for N<sub>2</sub>O and N<sub>2</sub> gas emissions from soils due to denitrification. *Global Biogeochemical Cycles*, *14*(4), 1045–1060. <https://doi.org/10.1029/1999GB001225>
- Deng, L., Huang, C., Kim, D., Shangguan, Z., Wang, K., Song, X., & Peng, C. (2020). Soil GHG fluxes are altered by N deposition: New data indicate lower N stimulation of the N<sub>2</sub>O flux and greater stimulation of the calculated C pools. *Global Change Biology*, *26*(4), 2613–2629. <https://doi.org/10.1111/gcb.14970>
- Dentener, F., Drevet, J., Lamarque, J. F., Bey, I., Eickhout, B., Fiore, A. M., et al. (2006). Nitrogen and sulfur deposition on regional and global scales: A multimodel evaluation. *Global Biogeochemical Cycles*, *20*(4), 2005GB002672. <https://doi.org/10.1029/2005GB002672>
- Dinsmore, K. J., Drewer, J., Levy, P. E., George, C., Lohila, A., Aurela, M., & Skiba, U. M. (2017). Growing season CH<sub>4</sub> and N<sub>2</sub>O fluxes from a subarctic landscape in northern Finland; from chamber to landscape scale. *Biogeosciences*, *14*(4), 799–815. <https://doi.org/10.5194/bg-14-799-2017>
- Drewer, J., Lohila, A., Aurela, M., Laurila, T., Minkinen, K., Penttilä, T., et al. (2010). Comparison of greenhouse gas fluxes and nitrogen budgets from an ombrotrophic bog in Scotland and a minerotrophic sedge fen in Finland. *European Journal of Soil Science*, *61*(5), 640–650. <https://doi.org/10.1111/j.1365-2389.2010.01267.x>
- Du, Y., Guo, X., Cao, G., Wang, B., Pan, G., & Liu, D. L. (2016). Simulation and prediction of nitrous oxide emission by the water and nitrogen management model on the Tibetan plateau. *Biochemical Systematics and Ecology*, *65*, 49–56. <https://doi.org/10.1016/j.bse.2016.02.002>
- Du, Y., Ke, X., Li, J., Wang, Y., Cao, G., Guo, X., & Chen, K. (2021). Nitrogen deposition increases global grassland N<sub>2</sub>O emission rates steeply: A meta-analysis. *Catena*, *199*, 105105. <https://doi.org/10.1016/j.catena.2020.105105>
- Elberling, B., Christiansen, H. H., & Hansen, B. U. (2010). Erratum: High nitrous oxide production from thawing permafrost. *Nature Geoscience*, *3*(7), 506. <https://doi.org/10.1038/ngeo893>
- Elyrs, A. S., Wang, J., Metwally, M. A. S., Cheng, Y., Zhang, J., Cai, Z., et al. (2021). Global gross nitrification rates are dominantly driven by soil carbon-to-nitrogen stoichiometry and total nitrogen. *Global Change Biology*, *27*(24), 6512–6524. <https://doi.org/10.1111/gcb.15883>
- Fowler, D., Coyle, M., Skiba, U., Sutton, M. A., Cape, J. N., Reis, S., et al. (2013). The global nitrogen cycle in the twenty-first century. *Philosophical Transactions of the Royal Society B: Biological Sciences*, *368*(1621), 20130164. <https://doi.org/10.1098/rstb.2013.0164>
- Frey, K. E., McClelland, J. W., Holmes, R. M., & Smith, L. C. (2007). Impacts of climate warming and permafrost thaw on the riverine transport of nitrogen and phosphorus to the Kara Sea. *Journal of Geophysical Research*, *112*(G4), 2006JG000369. <https://doi.org/10.1029/2006JG000369>
- Furon, A. C., Wagner-Riddle, C., Smith, C. R., & Warland, J. S. (2008). Wavelet analysis of wintertime and spring thaw CO<sub>2</sub> and N<sub>2</sub>O fluxes from agricultural fields. *Agricultural and Forest Meteorology*, *148*(8–9), 1305–1317. <https://doi.org/10.1016/j.agrformet.2008.03.006>
- Gao, W., Yao, Y., Liang, H., Song, L., Sheng, H., Cai, T., & Gao, D. (2019). Emissions of nitrous oxide from continuous permafrost region in the Daxing'an Mountains, Northeast China. *Atmospheric Environment*, *198*, 34–45. <https://doi.org/10.1016/j.atmosenv.2018.10.045>
- Gil, J., Pérez, T., Boering, K., Martikainen, P. J., & Biasi, C. (2017). Mechanisms responsible for high N<sub>2</sub>O emissions from subarctic permafrost peatlands studied via stable isotope techniques: Subarctic Tundra N<sub>2</sub>O Stable Isotopes. *Global Biogeochemical Cycles*, *31*(1), 172–189. <https://doi.org/10.1002/2015GB005370>
- Glatzel, S., & Stahr, K. (2001). Methane and nitrous oxide exchange in differently fertilised grassland in southern Germany. *Plant and Soil*, *231*(1), 21–35. <https://doi.org/10.1023/A:1010315416866>
- GLOBAL SOIL DATA TASK. (2000). *Global gridded surfaces of Selected Soil Characteristics (IGBP-DIS)*. ORNL Distributed Active Archive Center. <https://doi.org/10.3334/ORNLDAA/569>
- Goldberg, S. D., & Gebauer, G. (2009). Drought turns a Central European Norway spruce forest soil from an N<sub>2</sub>O source to a transient N<sub>2</sub>O sink. *Global Change Biology*, *15*(4), 850–860. <https://doi.org/10.1111/j.1365-2486.2008.01752.x>
- Gong, Y., Wu, J., Vogt, J., & Le, T. B. (2019). Warming reduces the increase in N<sub>2</sub>O emission under nitrogen fertilization in a boreal peatland. *Science of The Total Environment*, *664*, 72–78. <https://doi.org/10.1016/j.scitotenv.2019.02.012>
- Groffman, P. M., Hardy, J. P., Driscoll, C. T., & Fahey, T. J. (2006). Snow depth, soil freezing, and fluxes of carbon dioxide, nitrous oxide and methane in a northern hardwood forest. *Global Change Biology*, *12*(9), 1748–1760. <https://doi.org/10.1111/j.1365-2486.2006.01194.x>
- Grosse, G., Goetz, S., McGuire, A. D., Romanovsky, V. E., & Schuur, E. A. G. (2016). Changing permafrost in a warming world and feedbacks to the Earth system. *Environmental Research Letters*, *11*(4), 040201. <https://doi.org/10.1088/1748-9326/11/4/040201>
- Hansen, H. F. E., & Elberling, B. (2023). Spatial distribution of bioavailable inorganic nitrogen from thawing permafrost. *Global Biogeochemical Cycles*, *37*(2), e2022GB007589. <https://doi.org/10.1029/2022GB007589>

- Harden, J. W., Koven, C. D., Ping, C., Hugelius, G., David McGuire, A., Camill, P., et al. (2012). Field information links permafrost carbon to physical vulnerabilities of thawing. *Geophysical Research Letters*, *39*(15), 2012GL051958. <https://doi.org/10.1029/2012GL051958>
- Harris, I., Osborn, T. J., Jones, P., & Lister, D. (2020). Version 4 of the CRU TS monthly high-resolution gridded multivariate climate dataset. *Scientific Data*, *7*(1), 109. <https://doi.org/10.1038/s41597-020-0453-3>
- Heinzle, J., Kitzler, B., Zechmeister-Boltenstern, S., Tian, Y., Kwatoch Kengdo, S., Wanek, W., et al. (2023). Soil CH<sub>4</sub> and N<sub>2</sub>O response diminishes during decadal soil warming in a temperate mountain forest. *Agricultural and Forest Meteorology*, *329*, 109287. <https://doi.org/10.1016/j.agrformet.2022.109287>
- Hénault, C., Bizouard, F., Laville, P., Gabrielle, B., Nicoulaud, B., Germon, J. C., & Cellier, P. (2005). Predicting in situ soil N<sub>2</sub>O emission using NOE algorithm and soil database. *Global Change Biology*, *11*(1), 115–127. <https://doi.org/10.1111/j.1365-2486.2004.00879.x>
- Huang, Y., & Gerber, S. (2015). Global soil nitrous oxide emissions in a dynamic carbon-nitrogen model. *Biogeosciences*, *12*(21), 6405–6427. <https://doi.org/10.5194/bg-12-6405-2015>
- Hugelius, G., Loisel, J., Chadburn, S., Jackson, R. B., Jones, M., MacDonald, G., et al. (2020). Large stocks of peatland carbon and nitrogen are vulnerable to permafrost thaw. *Proceedings of the National Academy of Sciences*, *117*(34), 20438–20446. <https://doi.org/10.1073/pnas.1916387117>
- Hugelius, G., Ramage, J., Burke, E., Chatterjee, A., Smallman, T. L., Aalto, T., et al. (2024). Permafrost region greenhouse gas budgets suggest a weak CO<sub>2</sub> sink and CH<sub>4</sub> and N<sub>2</sub>O sources, but magnitudes differ between top-down and bottom-up methods. *Global Biogeochemical Cycles*, *38*(10), e2023GB007969. <https://doi.org/10.1029/2023GB007969>
- IPCC. (2013). In *Climate change 2013: The physical science basis. Contribution of working group I to the fifth assessment report of the intergovernmental panel on climate change*. T. F. Stocker (Eds.), Cambridge University Press, 1535. Retrieved from <https://www.ipcc.ch/report/ar5/wg1/>
- Jiang, C., Yu, G., Fang, H., Cao, G., & Li, Y. (2010). Short-term effect of increasing nitrogen deposition on CO<sub>2</sub>, CH<sub>4</sub> and N<sub>2</sub>O fluxes in an alpine meadow on the Qinghai-Tibetan Plateau, China. *Atmospheric Environment*, *44*(24), 2920–2926. <https://doi.org/10.1016/j.atmosenv.2010.03.030>
- Jones, B. M., Baughman, C. A., Romanovsky, V. E., Parsekian, A. D., Babcock, E. L., Stephani, E., et al. (2016). Presence of rapidly degrading permafrost plateaus in south-central Alaska. *The Cryosphere*, *10*(6), 2673–2692. <https://doi.org/10.5194/tc-10-2673-2016>
- Jones, S. K., Rees, R. M., Skiba, U. M., & Ball, B. C. (2005). Greenhouse gas emissions from a managed grassland. *Global and Planetary Change*, *47*(2–4), 201–211. <https://doi.org/10.1016/j.gloplacha.2004.10.011>
- Jørgensen, C. J., & Elberling, B. (2012). Effects of flooding-induced N<sub>2</sub>O production, consumption and emission dynamics on the annual N<sub>2</sub>O emission budget in wetland soil. *Soil Biology and Biochemistry*, *53*, 9–17. <https://doi.org/10.1016/j.soilbio.2012.05.005>
- Köster, E., Köster, K., Berninger, F., Aaltonen, H., Zhou, X., & Pumpanen, J. (2017). Carbon dioxide, methane and nitrous oxide fluxes from a fire chronosequence in subarctic boreal forests of Canada. *Science of The Total Environment*, *601–602*, 895–905. <https://doi.org/10.1016/j.scitotenv.2017.05.246>
- Kunhikrishnan, A., Thangarajan, R., Bolan, N. S., Xu, Y., Mandal, S., Gleeson, D. B., et al. (2016). Functional relationships of soil acidification, liming, and greenhouse gas flux. In *Advances in agronomy* (Vol. 139, pp. 1–71). Elsevier. <https://doi.org/10.1016/bs.agron.2016.05.001>
- Lacroix, F., Zaehle, S., Caldararu, S., Schaller, J., Stimmler, P., Holl, D., et al. (2022). Mismatch of N release from the permafrost and vegetative uptake opens pathways of increasing nitrous oxide emissions in the high Arctic. *Global Change Biology*, *28*(20), 5973–5990. <https://doi.org/10.1111/gcb.16345>
- Li, C., Frohling, S., & Frohling, T. A. (1992). A model of nitrous oxide evolution from soil driven by rainfall events: 2. Model applications. *Journal of Geophysical Research*, *97*(D9), 9777–9783. <https://doi.org/10.1029/92JD00510>
- Li, Y., Dong, S., Liu, S., Zhou, H., Gao, Q., Cao, G., et al. (2015). Seasonal changes of CO<sub>2</sub>, CH<sub>4</sub> and N<sub>2</sub>O fluxes in different types of alpine grassland in the Qinghai-Tibetan Plateau of China. *Soil Biology and Biochemistry*, *80*, 306–314. <https://doi.org/10.1016/j.soilbio.2014.10.026>
- Liu, L., Zhuang, Q., Zhao, D., Zheng, D., Kou, D., & Yang, Y. (2022). Permafrost degradation diminishes terrestrial ecosystem carbon sequestration capacity on the Qinghai-Tibetan plateau. *Global Biogeochemical Cycles*, *36*(2), e2021GB007068. <https://doi.org/10.1029/2021GB007068>
- Liu, X., Zhang, Q., Li, S., Zhang, L., & Ren, J. (2017). Simulated NH<sub>4</sub><sup>+</sup>-N deposition inhibits CH<sub>4</sub> uptake and promotes N<sub>2</sub>O emission in the meadow Steppe of inner Mongolia, China. *Pedosphere*, *27*(2), 306–317. [https://doi.org/10.1016/S1002-0160\(17\)60318-7](https://doi.org/10.1016/S1002-0160(17)60318-7)
- Lohila, A., Aurela, M., Hatakka, J., Pihlatie, M., Minkkinen, K., Penttilä, T., & Laurila, T. (2010). Responses of N<sub>2</sub>O fluxes to temperature, water table and N deposition in a northern boreal fen. *European Journal of Soil Science*, *61*(5), 651–661. <https://doi.org/10.1111/j.1365-2389.2010.01265.x>
- Ludwig, B., Teepe, R., Lopes De Gerenyu, V., & Flessa, H. (2006). CO<sub>2</sub> and N<sub>2</sub>O emissions from gleyic soils in the Russian tundra and a German forest during freeze–thaw periods—A microcosm study. *Soil Biology and Biochemistry*, *38*(12), 3516–3519. <https://doi.org/10.1016/j.soilbio.2006.06.006>
- Luo, G. J., Kiese, R., Wolf, B., & Butterbach-Bahl, K. (2013). Effects of soil temperature and moisture on methane uptake and nitrous oxide emissions across three different ecosystem types. *Biogeosciences*, *10*(5), 3205–3219. <https://doi.org/10.5194/bg-10-3205-2013>
- Ma, W. K., Schautz, A., Fishback, L.-A. E., Bedard-Haughn, A., Farrell, R. E., & Siciliano, S. D. (2007). Assessing the potential of ammonia oxidizing bacteria to produce nitrous oxide in soils of a high arctic lowland ecosystem on Devon Island, Canada. *Soil Biology and Biochemistry*, *39*(8), 2001–2013. <https://doi.org/10.1016/j.soilbio.2007.03.001>
- Maljanen, M., Alm, J., Martikainen, P. J., & Repo, T. (2010). Prolongation of soil frost resulting from reduced snow cover increases nitrous oxide emissions from boreal forest soil. *Boreal Environment Research*, *15*.
- Maljanen, M., Jokinen, H., Saari, A., Strömmer, R., & Martikainen, P. J. (2006). Methane and nitrous oxide fluxes, and carbon dioxide production in boreal forest soil fertilized with wood ash and nitrogen. *Soil Use & Management*, *22*(2), 151–157. <https://doi.org/10.1111/j.1475-2743.2006.00029.x>
- Martikainen, P. J., Nykänen, H., Crill, P., & Silvola, J. (1993). Effect of a lowered water table on nitrous oxide fluxes from northern peatlands. *Nature*, *366*(6450), 51–53. <https://doi.org/10.1038/366051a0>
- Marushchak, M. E., Kerttula, J., Diáková, K., Faguet, A., Gil, J., Grosse, G., et al. (2021). Thawing Yedoma permafrost is a neglected nitrous oxide source. *Nature Communications*, *12*(1), 7107. <https://doi.org/10.1038/s41467-021-27386-2>
- Marushchak, M. E., Pitkämäki, A., Koponen, H., Biasi, C., Seppälä, M., & Martikainen, P. J. (2011). Hot spots for nitrous oxide emissions found in different types of permafrost peatlands. *Global Change Biology*, *17*(8), 2601–2614. <https://doi.org/10.1111/j.1365-2486.2011.02442.x>
- Matson, A., Pennock, D., & Bedard-Haughn, A. (2009). Methane and nitrous oxide emissions from mature forest stands in the boreal forest, Saskatchewan, Canada. *Forest Ecology and Management*, *258*(7), 1073–1083. <https://doi.org/10.1016/j.foreco.2009.05.034>

- McClelland, J. W., Stieglitz, M., Pan, F., Holmes, R. M., & Peterson, B. J. (2007). Recent changes in nitrate and dissolved organic carbon export from the upper Kuparuk River, North Slope, Alaska. *Journal of Geophysical Research*, *112*(G4), 2006JG000371. <https://doi.org/10.1029/2006JG000371>
- McGuire, A. D., Christensen, T. R., Hayes, D., Heroult, A., Euskirchen, E., Kimball, J. S., et al. (2012). An assessment of the carbon balance of arctic tundra: Comparisons among observations, process models, and atmospheric inversions. *Biogeosciences*, *9*(8), 3185–3204. <https://doi.org/10.5194/bg-9-3185-2012>
- McGuire, A. D., Melillo, J. M., Kicklighter, D. W., Pan, Y., Xiao, X., Helfrich, J., et al. (1997). Equilibrium responses of global net primary production and carbon storage to doubled atmospheric carbon dioxide: Sensitivity to changes in vegetation nitrogen concentration. *Global Biogeochemical Cycles*, *11*(2), 173–189. <https://doi.org/10.1029/97GB00059>
- Melillo, J. M., McGuire, A. D., Kicklighter, D. W., Moore, B., Vorosmarty, C. J., & Schloss, A. L. (1993). Global climate change and terrestrial net primary production. *Nature*, *363*(6426), 234–240. <https://doi.org/10.1038/363234a0>
- Merbold, L., Steinlin, C., & Hagedorn, F. (2013). Winter greenhouse gas fluxes (CO<sub>2</sub>, CH<sub>4</sub> and N<sub>2</sub>O) from a subalpine grassland. *Biogeosciences*, *10*(5), 3185–3203. <https://doi.org/10.5194/bg-10-3185-2013>
- Mishra, U., Hugelius, G., Shelef, E., Yang, Y., Strauss, J., Lupachev, A., et al. (2021). Spatial heterogeneity and environmental predictors of permafrost region soil organic carbon stocks. *Science Advances*, *7*(9), eaaz5236. <https://doi.org/10.1126/sciadv.aaz5236>
- Monteux, S., Keuper, F., Fontaine, S., Gavazov, K., Hallin, S., Juhanson, J., et al. (2020). Carbon and nitrogen cycling in Yedoma permafrost controlled by microbial functional limitations. *Nature Geoscience*, *13*(12), 794–798. <https://doi.org/10.1038/s41561-020-00662-4>
- Morishita, T., Matsuura, Y., Kajimoto, T., Osawa, A., Zyryanova, O. A., & Prokushkin, A. S. (2014). CH<sub>4</sub> and N<sub>2</sub>O dynamics of a Larix gmelinii forest in a continuous permafrost region of central Siberia during the growing season. *Polar Science*, *8*(2), 156–165. <https://doi.org/10.1016/j.polar.2014.01.004>
- Natali, S. M., Holdren, J. P., Rogers, B. M., Treharne, R., Duffy, P. B., Pomerance, R., & MacDonald, E. (2021). Permafrost carbon feedbacks threaten global climate goals. *Proceedings of the National Academy of Sciences*, *118*(21), e2100163118. <https://doi.org/10.1073/pnas.2100163118>
- Obu, J. (2021). How much of the Earth's surface is underlain by permafrost? *Journal of Geophysical Research: Earth Surface*, *126*(5), e2021JF006123. <https://doi.org/10.1029/2021JF006123>
- Overland, J. E., Wang, M., Walsh, J. E., & Stroeve, J. C. (2014). Future Arctic climate changes: Adaptation and mitigation time scales. *Earth's Future*, *2*(2), 68–74. <https://doi.org/10.1002/2013EF000162>
- Palmtag, J., Obu, J., Kuhry, P., Richter, A., Siewert, M. B., Weiss, N., et al. (2022). A high spatial resolution soil carbon and nitrogen dataset for the northern permafrost region based on circumpolar land cover upscaling. *Earth System Science Data*, *14*(9), 4095–4110. <https://doi.org/10.5194/essd-14-4095-2022>
- Parton, W. J., Holland, E. A., Del Grosso, S. J., Hartman, M. D., Martin, R. E., Mosier, A. R., et al. (2001). Generalized model for NO<sub>x</sub> and N<sub>2</sub>O emissions from soils. *Journal of Geophysical Research*, *106*(D15), 17403–17419. <https://doi.org/10.1029/2001JD900101>
- Parton, W. J., Mosier, A. R., Ojima, D. S., Valentine, D. W., Schimel, D. S., Weier, K., & Kulmala, A. E. (1996). Generalized model for N<sub>2</sub> and N<sub>2</sub>O production from nitrification and denitrification. *Global Biogeochemical Cycles*, *10*(3), 401–412. <https://doi.org/10.1029/96GB01455>
- Pedersen, E. P., Elberling, B., & Michelsen, A. (2020). Foraging deeply: Depth-specific plant nitrogen uptake in response to climate-induced N-release and permafrost thaw in the High Arctic. *Global Change Biology*, *26*(11), 6523–6536. <https://doi.org/10.1111/gcb.15306>
- Post, E., Alley, R. B., Christensen, T. R., Macias-Fauria, M., Forbes, B. C., Gooseff, M. N., et al. (2019). The polar regions in a 2°C warmer world. *Science Advances*, *5*(12), eaaw9883. <https://doi.org/10.1126/sciadv.aaw9883>
- Post, W. M., Pastor, J., Zinke, P. J., & Stangenberger, A. G. (1985). Global patterns of soil nitrogen storage. *Nature*, *317*(6038), 613–616. <https://doi.org/10.1038/317613a0>
- Potter, C. S., Matson, P. A., Vitousek, P. M., & Davidson, E. A. (1996). Process modeling of controls on nitrogen trace gas emissions from soils worldwide. *Journal of Geophysical Research*, *101*(D1), 1361–1377. <https://doi.org/10.1029/95JD02028>
- Qin, Z., Zhuang, Q., & Zhu, X. (2014). Carbon and nitrogen dynamics in bioenergy ecosystems: 1. Model development, validation and sensitivity analysis. *GCB Bioenergy*, *6*(6), 740–755. <https://doi.org/10.1111/gcbb.12107>
- Qin, Z., Zhuang, Q., & Zhu, X. (2015). Carbon and nitrogen dynamics in bioenergy ecosystems: 2. Potential greenhouse gas emissions and global warming intensity in the conterminous United States. *GCB Bioenergy*, *7*(1), 25–39. <https://doi.org/10.1111/gcbb.12106>
- Ramage, J., Kuhn, M., Virkkala, A., Voigt, C., Marushchak, M. E., Bastos, A., et al. (2024). The net GHG balance and budget of the permafrost region (2000–2020) from ecosystem flux upscaling. *Global Biogeochemical Cycles*, *38*(4), e2023GB007953. <https://doi.org/10.1029/2023GB007953>
- Ravishankara, A. R., Daniel, J. S., & Portmann, R. W. (2009). Nitrous oxide (N<sub>2</sub>O): The dominant ozone-depleting substance emitted in the 21st century. *Science*, *326*(5949), 123–125. <https://doi.org/10.1126/science.1176985>
- R Core Team. (2024). *R: A language and environment for statistical computing*. Version 4.3.3. R Foundation for Statistical Computing. Retrieved from <https://www.R-project.org/>
- Repo, M. E., Susiluoto, S., Lind, S. E., Jokinen, S., Elsakov, V., Biasi, C., et al. (2009). Large N<sub>2</sub>O emissions from cryoturbated peat soil in tundra. *Nature Geoscience*, *2*(3), 189–192. <https://doi.org/10.1038/ngeo434>
- Risk, N., Snider, D., & Wagner-Riddle, C. (2013). Mechanisms leading to enhanced soil nitrous oxide fluxes induced by freeze–thaw cycles. *Canadian Journal of Soil Science*, *93*(4), 401–414. <https://doi.org/10.4141/cjss2012-071>
- Romanovsky, V. E., Smith, S. L., & Christiansen, H. H. (2010). Permafrost thermal state in the polar northern hemisphere during the international polar year 2007–2009: A synthesis. *Permafrost and Periglacial Processes*, *21*(2), 106–116. <https://doi.org/10.1002/ppp.689>
- Röver, M., Heinemeyer, O., & Kaiser, E.-A. (1998). Microbial induced nitrous oxide emissions from an arable soil during winter. *Soil Biology and Biochemistry*, *30*(14), 1859–1865. [https://doi.org/10.1016/S0038-0717\(98\)00080-7](https://doi.org/10.1016/S0038-0717(98)00080-7)
- Saikawa, E., Schlosser, C. A., & Prinn, R. G. (2013). Global modeling of soil nitrous oxide emissions from natural processes. *Global Biogeochemical Cycles*, *27*(3), 972–989. <https://doi.org/10.1002/gbc.20087>
- Salmon, V. G., Soucy, P., Mauritz, M., Celis, G., Natali, S. M., Mack, M. C., & Schuur, E. A. G. (2016). Nitrogen availability increases in a tundra ecosystem during five years of experimental permafrost thaw. *Global Change Biology*, *22*(5), 1927–1941. <https://doi.org/10.1111/gcb.13204>
- Schlesinger, W. H. (2013). An estimate of the global sink for nitrous oxide in soils. *Global Change Biology*, *19*(10), 2929–2931. <https://doi.org/10.1111/gcb.12239>
- Schuur, E. A. G., & Abbott, B. (2011). High risk of permafrost thaw. *Nature*, *480*(7375), 32–33. <https://doi.org/10.1038/480032a>
- Shan, J., Sanford, R. A., Chee-Sanford, J., Ooi, S. K., Löffler, F. E., Konstantinidis, K. T., & Yang, W. H. (2021). Beyond denitrification: The role of microbial diversity in controlling nitrous oxide reduction and soil nitrous oxide emissions. *Global Change Biology*, *27*(12), 2669–2683. <https://doi.org/10.1111/gcb.15545>

- Sierra, C. A., Trumbore, S. E., Davidson, E. A., Vicca, S., & Janssens, I. (2015). Sensitivity of decomposition rates of soil organic matter with respect to simultaneous changes in temperature and moisture. *Journal of Advances in Modeling Earth Systems*, 7(1), 335–356. <https://doi.org/10.1002/2014MS000358>
- Siljanen, H. M. P., Alves, R. J. E., Ronkainen, J. G., Lamprecht, R. E., Bhattarai, H. R., Bagnoud, A., et al. (2019). Archaeal nitrification is a key driver of high nitrous oxide emissions from arctic peatlands. *Soil Biology and Biochemistry*, 137, 107539. <https://doi.org/10.1016/j.soilbio.2019.107539>
- Siljanen, H. M. P., Welti, N., Voigt, C., Heiskanen, J., Biasi, C., & Martikainen, P. J. (2020). Atmospheric impact of nitrous oxide uptake by boreal forest soils can be comparable to that of methane uptake. *Plant and Soil*, 454(1–2), 121–138. <https://doi.org/10.1007/s11104-020-04638-6>
- Smith, K. A., Thomson, P. E., Clayton, H., McTaggart, I. P., & Conen, F. (1998). Effects of temperature, water content and nitrogen fertilisation on emissions of nitrous oxide by soils. *Atmospheric Environment*, 32(19), 3301–3309. [https://doi.org/10.1016/S1352-2310\(97\)00492-5](https://doi.org/10.1016/S1352-2310(97)00492-5)
- Strauss, J., Biasi, C., Sanders, T., Abbott, B. W., Von Deimling, T. S., Voigt, C., et al. (2022). A globally relevant stock of soil nitrogen in the Yedoma permafrost domain. *Nature Communications*, 13(1), 6074. <https://doi.org/10.1038/s41467-022-33794-9>
- Syakila, A., & Kroeze, C. (2011). The global nitrous oxide budget revisited. *Greenhouse Gas Measurement and Management*, 1(1), 17–26. <https://doi.org/10.3763/ghgmm.2010.0007>
- Takakai, F., Desyatkin, A. R., Lopez, C. M. L., Fedorov, A. N., Desyatkin, R. V., & Hatano, R. (2008). CH<sub>4</sub> and N<sub>2</sub>O emissions from a forest-alas ecosystem in the permafrost taiga forest region, eastern Siberia, Russia. *Journal of Geophysical Research*, 113(G2), 2007JG000521. <https://doi.org/10.1029/2007JG000521>
- Tao, J., Koster, R. D., Reichle, R. H., Forman, B. A., Xue, Y., Chen, R. H., & Moghaddam, M. (2019). Permafrost variability over the Northern Hemisphere based on the MERRA-2 reanalysis. *The Cryosphere*, 13(8), 2087–2110. <https://doi.org/10.5194/tc-13-2087-2019>
- Teepe, R., Brumme, R., Beese, F., & Ludwig, B. (2004). Nitrous oxide emission and methane consumption following compaction of forest soils. *Soil Science Society of America Journal*, 68(2), 605–611. <https://doi.org/10.2136/sssaj2004.6050>
- Teepe, R., Vor, A., Beese, F., & Ludwig, B. (2004). Emissions of N<sub>2</sub>O from soils during cycles of freezing and thawing and the effects of soil water, texture and duration of freezing. *European Journal of Soil Science*, 55(2), 357–365. <https://doi.org/10.1111/j.1365-2389.2004.00602.x>
- Tian, H., Xu, R., Canadell, J. G., Thompson, R. L., Winiwarter, W., Suntharalingam, P., et al. (2020). A comprehensive quantification of global nitrous oxide sources and sinks. *Nature*, 586(7828), 248–256. <https://doi.org/10.1038/s41586-020-2780-0>
- Ullah, S., & Moore, T. R. (2011). Biogeochemical controls on methane, nitrous oxide, and carbon dioxide fluxes from deciduous forest soils in eastern Canada. *Journal of Geophysical Research*, 116(G3), G03010. <https://doi.org/10.1029/2010JG001525>
- Van Bochove, E., Bertrand, N., & Caron, J. (1998). In situ estimation of the gaseous nitrous oxide diffusion coefficient in a sandy loam soil. *Soil Science Society of America Journal*, 62(5), 1178–1184. <https://doi.org/10.2136/sssaj1998.03615995006200050004x>
- Vishwakarma, S., Zhang, X., Dobermann, A., Heffer, P., & Zhou, F. (2023). Global nitrogen deposition inputs to cropland at national scale from 1961 to 2020. *Scientific Data*, 10(1), 488. <https://doi.org/10.1038/s41597-023-02385-8>
- Voigt, C., Lamprecht, R. E., Marushchak, M. E., Lind, S. E., Novakovskiy, A., Aurela, M., et al. (2017). Warming of subarctic tundra increases emissions of all three important greenhouse gases - Carbon dioxide, methane, and nitrous oxide. *Global Change Biology*, 23(8), 3121–3138. <https://doi.org/10.1111/gcb.13563>
- Voigt, C., Marushchak, M. E., Abbott, B. W., Biasi, C., Elberling, B., Siciliano, S. D., et al. (2020). Nitrous oxide emissions from permafrost-affected soils. *Nature Reviews Earth and Environment*, 1(8), 420–434. <https://doi.org/10.1038/s43017-020-0063-9>
- Wagena, M. B., Bock, E. M., Sommerlot, A. R., Fuka, D. R., & Easton, Z. M. (2017). Development of a nitrous oxide routine for the SWAT model to assess greenhouse gas emissions from agroecosystems. *Environmental Modelling and Software*, 89, 131–143. <https://doi.org/10.1016/j.envsoft.2016.11.013>
- Wagner, I., Hung, J. K. Y., Neil, A., & Scott, N. A. (2019). Net greenhouse gas fluxes from three High Arctic plant communities along a moisture gradient. *Arctic Science*, 5(4), 185–201. <https://doi.org/10.1139/as-2018-0018>
- Wagner-Riddle, C., Hu, Q. C., Van Bochove, E., & Jayasundara, S. (2008). Linking nitrous oxide flux during spring thaw to nitrate denitrification in the soil profile. *Soil Science Society of America Journal*, 72(4), 908–916. <https://doi.org/10.2136/sssaj2007.0353>
- Wen, Y., Chen, Z., Dannenmann, M., Carminati, A., Willibald, G., Kiese, R., et al. (2016). Disentangling gross N<sub>2</sub>O production and consumption in soil. *Scientific Reports*, 6(1), 36517. <https://doi.org/10.1038/srep36517>
- Wen, Y., Corre, M. D., Rachow, C., Chen, L., & Veldkamp, E. (2017). Nitrous oxide emissions from stems of alder, beech and spruce in a temperate forest. *Plant and Soil*, 420(1–2), 423–434. <https://doi.org/10.1007/s11104-017-3416-5>
- Wrage, N., Velthof, G. L., Laanbroek, H. J., & Oenema, O. (2004). Nitrous oxide production in grassland soils: Assessing the contribution of nitrifier denitrification. *Soil Biology and Biochemistry*, 36(2), 229–236. <https://doi.org/10.1016/j.soilbio.2003.09.009>
- Wu, X., Brüggemann, N., Gasche, R., Shen, Z., Wolf, B., & Butterbach-Bahl, K. (2010). Environmental controls over soil-atmosphere exchange of N<sub>2</sub>O, NO, and CO<sub>2</sub> in a temperate Norway spruce forest. *Global Biogeochemical Cycles*, 24(2). <https://doi.org/10.1029/2009GB003616>
- Wu, X., Zang, S., Ma, D., Ren, J., Chen, Q., & Dong, X. (2019). Emissions of CO<sub>2</sub>, CH<sub>4</sub>, and N<sub>2</sub>O fluxes from forest soil in permafrost region of daxing' an mountains, Northeast China. *International Journal of Environmental Research and Public Health*, 16(16), 2999. <https://doi.org/10.3390/ijerph16162999>
- Xiao, R., Ran, W., Hu, S., & Guo, H. (2021). The response of ammonia oxidizing archaea and bacteria in relation to heterotrophs under different carbon and nitrogen amendments in two agricultural soils. *Applied Soil Ecology*, 158, 103812. <https://doi.org/10.1016/j.apsoil.2020.103812>
- Xu, W., Frendrup, L. L., Michelsen, A., Elberling, B., & Ambus, P. L. (2023). Deepened snow in combination with summer warming increases growing season nitrous oxide emissions in dry tundra, but not in wet tundra. *Soil Biology and Biochemistry*, 180, 109013. <https://doi.org/10.1016/j.soilbio.2023.109013>
- Yan, Y., Ganjurjav, H., Hu, G., Liang, Y., Li, Y., He, S., et al. (2018). Nitrogen deposition induced significant increase of N<sub>2</sub>O emissions in a dry alpine meadow on the central Qinghai–Tibetan Plateau. *Agriculture, Ecosystems and Environment*, 265, 45–53. <https://doi.org/10.1016/j.agee.2018.05.031>
- Yang, W. H., & Silver, W. L. (2016). Net soil–atmosphere fluxes mask patterns in gross production and consumption of nitrous oxide and methane in a managed ecosystem. *Biogeosciences*, 13(5), 1705–1715. <https://doi.org/10.5194/bg-13-1705-2016>
- Yang, Z., Ou, Y. H., Xu, X., Zhao, L., Song, M., & Zhou, C. (2010). Effects of permafrost degradation on ecosystems. *Acta Ecologica Sinica*, 30(1), 33–39. <https://doi.org/10.1016/j.chnaes.2009.12.006>
- Yu, T., & Zhuang, Q. (2019). Quantifying global N<sub>2</sub>O emissions from natural ecosystem soils using trait-based biogeochemistry models. *Biogeosciences*, 16(2), 207–222. <https://doi.org/10.5194/bg-16-207-2019>
- Yuan, Y., Zhuang, Q., Zhao, B., & Shurpali, N. J. (2023). Modeling N<sub>2</sub>O emission from the pan-Arctic terrestrial ecosystems [Dataset]. *Purdue University Research Repository*. <https://doi.org/10.4231/KZ5W-DC21>
- Yuan, Y., Zhuang, Q., Zhao, B., & Shurpali, N. J. (2025). Modeling N<sub>2</sub>O emission from the pan-Arctic terrestrial ecosystems (Version 2.0) [Dataset]. *Purdue University Research Repository*. <https://doi.org/10.4231/STN5-2979>

- Zhao, B., & Zhuang, Q. (2024). Nitrogen cycling feedback on carbon dynamics leads to greater CH<sub>4</sub> emissions and weaker cooling effect of northern Peatlands. *Global Biogeochemical Cycles*, 38(4), e2023GB007978. <https://doi.org/10.1029/2023GB007978>
- Zhou, Y., Hagedorn, F., Zhou, C., Jiang, X., Wang, X., & Li, M.-H. (2016). Experimental warming of a mountain tundra increases soil CO<sub>2</sub> effluxes and enhances CH<sub>4</sub> and N<sub>2</sub>O uptake at Changbai Mountain, China. *Scientific Reports*, 6(1), 21108. <https://doi.org/10.1038/srep21108>
- Zhu, R., Chen, Q., Ding, W., & Xu, H. (2012). Impact of seabird activity on nitrous oxide and methane fluxes from High Arctic tundra in Svalbard, Norway. *Journal of Geophysical Research*, 117(G4), 2012JG002130. <https://doi.org/10.1029/2012JG002130>
- Zhuang, Q., McGUIRE, A. D., Melillo, J. M., Clein, J. S., Dargaville, R. J., Kicklighter, D. W., et al. (2003). Carbon cycling in extratropical terrestrial ecosystems of the Northern Hemisphere during the 20th century: A modeling analysis of the influences of soil thermal dynamics. *Tellus B: Chemical and Physical Meteorology*, 55(3), 751–776. <https://doi.org/10.1034/j.1600-0889.2003.00060.x>
- Zhuang, Q., Romanovsky, V. E., & McGuire, A. D. (2001). Incorporation of a permafrost model into a large-scale ecosystem model: Evaluation of temporal and spatial scaling issues in simulating soil thermal dynamics. *Journal of Geophysical Research*, 106(D24), 33649–33670. <https://doi.org/10.1029/2001JD900151>